



HAL
open science

Oceanic mercury concentrations on both sides of the Strait of Gibraltar decreased between 1989 and 2012

Daniel Cossa, Joël Knoery, Marie Boye, Nicolas Maruszczak, Bastien Thomas, Philippe Courau, Francesca Sprovieri

► **To cite this version:**

Daniel Cossa, Joël Knoery, Marie Boye, Nicolas Maruszczak, Bastien Thomas, et al.. Oceanic mercury concentrations on both sides of the Strait of Gibraltar decreased between 1989 and 2012. *Anthropocene*, 2020, ANTRHOPOCENE, 29, pp.100230. 10.1016/j.ancene.2019.100230 . hal-02384726

HAL Id: hal-02384726

<https://hal.science/hal-02384726>

Submitted on 28 Nov 2019

HAL is a multi-disciplinary open access archive for the deposit and dissemination of scientific research documents, whether they are published or not. The documents may come from teaching and research institutions in France or abroad, or from public or private research centers.

L'archive ouverte pluridisciplinaire **HAL**, est destinée au dépôt et à la diffusion de documents scientifiques de niveau recherche, publiés ou non, émanant des établissements d'enseignement et de recherche français ou étrangers, des laboratoires publics ou privés.

1 **Oceanic mercury concentrations on both sides of the Strait of Gibraltar**
2 **decreased between 1989 and 2012**

3 **Daniel Cossa (1,2), Joël Knoery (2), Marie Boye (3), Nicolas Maruszczak (2), Bastien**
4 **Thomas (2), Philippe Courau (4), Francesca Sprovieri (5)**

4 1. ISTerre, Université Grenoble Alpes, BP 53, F-38041 Grenoble, France
2. IFREMER, Atlantic Center, LBCM, F-44031 Nantes, France
3. Institut de Physique du Globe de Paris, Université de Paris, F-75238 Paris, France 4. CNRS, LOV, F-06230 Villefranche-sur-Mer, France
5. CNR, Institute of Atmospheric Pollution Research, I-87036 Rende, Italy

5 **Abstract**

6 *Mercury (Hg) is a toxic metal that threatens the health of aquatic ecosystems and fish*
7 *consumers. Its natural cycle has been deeply perturbed by anthropogenic Hg emissions,*
8 *especially since the start of the Industrial Revolution circa 1850 AD. Anthropogenic Hg*
9 *emissions from North America and Europe have decreased by a factor of two in the last*
10 *decades following the implementation of strict regulations. The response of North Atlantic*
11 *Ocean and Mediterranean waters to this decrease remains poorly documented by field*
12 *observations. A comparison of results obtained between 1989 and 2012 shows a significant*
13 *decrease of Hg concentrations in waters on both sides of the Strait of Gibraltar. West of*
14 *Gibraltar, the Hg decrease ranges from ~35% in the upper North East Atlantic Deep Water*
15 *to ~50% in the North East Atlantic Central Water. East of Gibraltar, the observed decrease*
16 *is ~30% in the Western Mediterranean Deep Water. No decrease is observed in the deep*
17 *Atlantic Ocean layer that formed before the industrial era. Our results strongly substantiate*
18 *the effectiveness of global anti-pollution policies on Hg contamination in oceanic waters. A*
19 *consequent decline of Hg bioaccumulation in Northeastern Atlantic and Western*
20 *Mediterranean pelagic ecosystems is still to be verified.*

21

22 **Keywords:** *Mercury, Mediterranean Sea, Atlantic Ocean, Gibraltar*

23

24 1. Introduction

25 Mercury (Hg) is a trace element which affects human health primarily *via* marine fish
26 consumption (e.g., Fitzgerald et al., 2007). Its toxicity is essentially due to the presence of
27 methylmercury (MeHg), which biomagnifies up food webs (e.g., Clarkson and Magos, 2006).
28 In aquatic environments, MeHg is formed by methylation of inorganic Hg by microorganisms
29 (e.g., Jensen and Jernelöv, 1969; Parks et al., 2013). In the open ocean, although MeHg
30 formation has been shown in sub-surface seawater and sediments (e.g., Monperrus et al.,
31 2007; Hollweg et al., 2010; Soerensen et al., 2016), it occurs mainly in the
32 thermocline/intermediate waters (200-1000 m) where most bacterial organic matter
33 regeneration occurs (e.g., Mason and Fitzgerald, 1990; Cossa et al., 2009; Blum et al., 2013;
34 Cossa et al., 2017). Inorganic Hg reaches the thermocline/intermediate waters *via* the
35 solubility and biological pumps (e.g., Fitzgerald and Lamborg, 2003; Mason et al., 2012;
36 Lamborg et al., 2016; Semeniuk and Dastoor, 2017). The solubility pump advects Hg with
37 water circulation, while the biological pump transports Hg to deep water with sinking
38 biogenic debris after its adsorption/uptake by phytoplankton in the upper reaches of the water
39 column. At thermocline/intermediate levels, inorganic Hg associated with particulate matter
40 is partially dissolved during the remineralization of organic matter and used as a substrate by
41 microorganisms for MeHg synthesis. Since direct atmospheric Hg deposition represents the
42 principal source of inorganic Hg to the open ocean (e.g., Mason et al., 2012; Sonke et al.,
43 2013), its rates of deposition and transport to thermocline/intermediate layer depths are, along
44 with the intensity of microbial activity there, the primary control factors on Hg methylation.
45 Ultimately, these parameters control the exposition of the base of the aquatic food web to
46 MeHg levels and thus constrain human contamination from seafood resources.

47 The Hg natural biogeochemical cycle has been disrupted by human activities for
48 several millennia (e.g., Cooke et al., 2009; Elbaz-Poulichet et al., 2011; Mason et al., 2012).

49 According to Amos et al. (2013), simulations show that the present-day Hg concentration in
50 the atmosphere is enriched by a factor of 2.6 relative to pre-industrial times (before ~1850
51 AD) and by a factor of 7.5 relative to natural levels. A recent critical review concludes that
52 atmospheric Hg concentrations have risen by about 4.5 times above the level prevailing
53 before 1450 AD (Outridge et al., 2018), and that this increase has driven a 3-fold increase in
54 the average deposition rates to the Earth's surface, which in turn has elevated Hg levels in
55 oceanic waters. Mass balance calculations suggest that within the last century Hg increased
56 by ~200% in the surface ocean, ~25% in subsurface waters, and ~10% in recently formed
57 deep waters (Mason et al., 2012). Modelling oceanic Hg changes in the last millennium
58 (Zhang et al., 2014a and b) suggests a Hg increase by a factor of 4.4 in the ocean mixed layer,
59 whereas the inventory of Hg has increased by 50 and 20% in the thermocline/intermediate
60 and deep ocean, respectively. Using a different approach, Lamborg et al. (2014a) calculated
61 that Hg concentrations have increased by 250%, 160% and 10% in surface,
62 thermocline/intermediate, and deep waters. They argue that these 3 layers contain
63 respectively 6%, 59% and 35% of total oceanic anthropogenic Hg. These figures are
64 comparable with the values of 3% in surface, 52% at thermocline/intermediate depths, and
65 45% for the deep ocean estimated by Zhang et al. (2014b). For their part, Outridge et al.
66 (2018), in their updated global and oceanic Hg budget, suggest that the oceanic Hg
67 concentrations increased compared to natural level by a factor of 2.3 in surface waters and by
68 only 12-25% in deeper layers. In addition, global Hg emissions, as well as the deposition
69 rates, are geographically heterogeneous, and the time-trends of Hg change in oceanic waters
70 are consequently geographically dependent (Mason et al., 2012; Lamborg et al. 2014b). For
71 example, the waters of the Pacific Ocean show a Hg increase at depths between 200 and 1000
72 m during the last few decades, while such a trend is not observed from measurements for
73 North Atlantic waters (Mason et al., 2012). Irrespective of the uncertainties of these various

74 estimates, all previously quoted studies converge in establishing that the anthropogenic
75 emissions of Hg and subsequent oceanic loading have massively increased since the
76 beginning of the industrial time. These anthropogenic perturbations will persist for years to
77 centuries depending on the geographical position and oceanic layer concerned. An insight of
78 the relative persistence of anthropogenic Hg can be derived from the residence times of Hg,
79 which are roughly < 1 year in the mixed layer (Soerensen et al., 2010), ~120 years in the
80 thermocline/intermediate layer, and ~2000 years in deep layers (Zhang et al., 2014b).

81 Observations in recent years of Hg concentrations in the atmosphere contrast with the
82 long-term assessments. Indeed, the Hg concentrations in the troposphere of the northern
83 hemisphere and the wet deposition have declined by ~35% during the 1990-2010 period
84 (Prestbo and Gay, 2009; Slemr et al., 2011; Muntean et al., 2014). More specifically, a
85 temporal decrease of Hg concentrations in the marine boundary layer of the North Atlantic
86 atmosphere was observed during the same period (Sprovieri et al., 2010; Cole and Steffen,
87 2010; Mao and Talbot, 2012; Weigelt et al., 2014). Zhang et al. (2016) reviewing the recent
88 atmospheric data conclude that the decrease in atmospheric elemental Hg (Hg^0)
89 concentrations ranges from 1.2 to 2.1 percent per year at northern midlatitudes, and that wet
90 deposition fluxes follow these trends. Similar observations for the oceanic waters are lacking
91 due to the sheer difficulty in obtaining an adequately long time series of quality Hg
92 concentration data (in both precision and accuracy) Hg concentration data. For an example, a
93 set of four measurements, obtained between 1980 and 2010, tends to suggest that surface
94 concentrations in the North Atlantic have decreased since the 1980s (Fig. 4 *in* Driscoll et al.,
95 2013). These data are obviously limited in their ability to provide a basis for sound
96 conclusions. For instance, the compilation of a larger dataset collected in the water column of
97 the North Atlantic Ocean near Bermuda (Fig. 4b *in* Mason et al., 2012) conversely does not
98 show a clear Hg decrease either at the surface or in intermediate or deep waters when early

99 data (i.e., the samples collected in 1979 that may be poorly validated) are excluded. Mercury
100 concentrations in the Eastern North Atlantic measured at the beginning of the 2000s (Cossa et
101 al., 2004) and in 2014 during a GEOTRACES cruise (Cossa et al., 2018a) are difficult to
102 compare because the data were obtained using different techniques for total Hg
103 determination. Indeed, the former method (hydride formation) is different from the now
104 validated bromine oxidation and tin chloride method (see Materials and Methods section)
105 which is widely used and considered as *the* reference method by research programs and many
106 national and international agencies. Nevertheless, this comparison suggests a decrease in Hg
107 concentration in the Mediterranean waters in recent decades, which has also been argued by
108 Rajar et al. (2007) by using data partially obtained by the hydride technique (Cossa et al.,
109 1997). Those decreases in the Mediterranean waters are consistent with the decrease of
110 American and European Hg emissions (Streets et al., 2009; Pirrone et al., 2010). However,
111 bearing in mind the uncertainty associated with the accuracy of early data, the observed
112 decreasing trend and its magnitude is questionable. Despite these trends in marine waters
113 being expected and predicted by modelling (Sunderland and Mason, 2007; Soerensen et al.,
114 2012), they need to be confirmed by unambiguous field data acquired using consistent
115 sampling and analytical techniques. Tentatively, a decrease by 30% in Hg concentrations is
116 observed when using the same sampling procedure and analytical method in the North
117 Atlantic (GEOTRACES GA-01 transect conducted in June 2014) between a recently formed
118 core (1-3 years) of the Labrador Sea Water (LSW) and a core of LSW of 20 years old (Cossa
119 et al. 2018a). Thus, additional field measurements are still clearly needed to actually observe
120 and confirm the probable but still hypothetical decrease in Hg burden of the North Atlantic
121 Ocean, both on a regional and seasonal basis. This latter is all the more important since
122 biological pumping and net Hg deposition rates are geographically variable (Mason et al.,
123 2012, 2017).

124 The Hg transfer at depth by biological pumping and Hg residence time at
125 thermocline/intermediate layers of the global ocean (~120 years) suggest that these oceanic
126 layers are the most suitable for investigating possible effects of changes in Hg deposition
127 over scale of a century. In addition, the upper layers of the North Atlantic and the entire water
128 column of the Western Mediterranean are also suitable water masses for studying decadal
129 environmental changes, since their residence time are of the order of two decades
130 (Cunningham, 2000; Béthoux et al., 2005, Schneider et al., 2014).

131 In this context, we are herein reporting the results of Hg determinations in the water
132 column, obtained during oceanographic cruises conducted on both sides of the Strait of
133 Gibraltar over the last 25 years using similar sampling and analytical techniques. The water
134 column west of Gibraltar is included in the Subtropical North Atlantic Gyre (STG), which is
135 one of the main features of North Atlantic circulation, and which anticyclonically links the
136 Gulf Stream to the North Equatorial Current. The STG is a region where subtropical and
137 recently ventilated waters mix, leading to an overturning of North Atlantic circulation
138 (Carracedo Segade et al., 2015). The water column east of Gibraltar, the so-called Alboran
139 Sea, contains the typical water masses of the Western Mediterranean (Millot et al., 2006;
140 Garcia-Lafuente et al., 2017) characterized by high salinity values due to evaporation which
141 exceeds precipitation reaching its maximum, particularly during summer. The Alboran Sea
142 constitutes the reservoir of Mediterranean outflow to the North Atlantic through the Strait of
143 Gibraltar. The objective of our study is answering the question: whether or not the decrease in
144 atmospheric Hg concentrations at northern midlatitudes, at the turn of the century, has had a
145 measurable impact on the Hg content of the water column of Northeast Atlantic and Western
146 Mediterranean both sides of the Strait of Gibraltar. We show that a significant decrease in Hg
147 concentrations occurs, between 1989 and 2012, in the upper and intermediate oceanic waters
148 on both sides of the Strait of Gibraltar.

150 2. Material and Methods

151 Samples were collected during three different cruises, MEDATLANTE-II in September 1989,
152 ALMOFRONT-I in May 1991, and FENICE in August 2012. The first two cruises were on board
153 the French research vessel “Jean Charcot” and the FENICE cruise was on board the Italian
154 research vessel “Urania” of the CNR (National Research Council). Two stations were
155 occupied west of Gibraltar: Sta. 6A during the MEDATLANTE-II cruise and Sta. 6B during the
156 FENICE cruise (Fig. 1). Three stations were occupied in the Alboran Sea: Stas. 36, 63 and 65
157 during the ALMOFRONT-I cruise, and Stas. 4 and 8 during the FENICE cruise.

158 Water samples were collected using the most state-of-the-art techniques for ultra-trace
159 Hg sampling and analysis that were available at the time of the cruises (Gill and Fitzgerald,
160 1985; Cossa and Courau, 1990; Mason and Fitzgerald, 1993; Yoon et al., 1996; Lamborg et
161 al., 2012). During ALMOFRONT-I and MEDATLANTE-II cruises, stainless-steel rosette frame
162 and hydrowire were deployed with acid-cleaned, Teflon-coated Go-Flo bottles (General
163 Oceanics), whereas, during FENICE cruise, Niskin bottles (General Oceanics) placed on an
164 epoxy-coated rosette and hung on a stainless steel hydrowire were used. During all three
165 cruises, the rosettes were equipped with sensors for salinity, temperature, dissolved oxygen,
166 and optical transmission. Samples for HgT determinations were treated and measured on
167 board from sub-samples, using identical procedures in clean lab-vans (Class 100000-ISO8
168 equipped with Class 100-ISO5 laminar flow hoods). Samples were withdrawn from sampling
169 bottles into acid-cleaned Teflon bottles (FEP), then stored acidified (Ultrapur HCl, 0.4% v/v)
170 until analysis, which was always performed within the next 12 hours. In order to determine
171 operationally defined total mercury (HgT) in the sample, Hg was released from its ligands
172 and alkyl moieties through oxidation with BrCl. Dissolved, oxidized Hg was reduced to its

173 Hg vapor with an acidic SnCl₂ solution. This technique, initially proposed by Bloom and
174 Crecelius (1983), is now known as the US-EPA standard method N° 1631 (EPA, 2002). For
175 our analyses, the Hg vapor is purged using Ar and amalgamated on a gold trap, then released
176 by thermal desorption into an atomic fluorescence spectrometer (Merlin, PSA in 1989-91,
177 and Tekran, Model 2500 in 2012). The detailed procedure for 1989-91 analyses is given by
178 Courau (1983), and by Cossa et al. (2018b) for 2012 analyses. The differences between
179 cruises are the following: in 1989-91, 125 mL of seawater sample was oxidized with the
180 bromide present in the seawater by the addition of 0.25 mL of a 0.04 mol L⁻¹ potassium
181 permanganate solution, then the Hg was reduced with 1 mL of a 0.05 M SnCl₂ solution. In
182 2012, the 100mL seawater subsample was oxidized with the addition of 0.1 mL of a 0.2 M
183 BrCl solution, and Hg reduction was achieved by 0.2 mL of a 1 M SnCl₂ solution. The
184 detection limit, defined at three times the standard deviation of six blank measurements, was
185 0.2 pmol L⁻¹ and 0.1 pmol L⁻¹ in 1989-91 and 2012, respectively. The reproducibility, defined
186 as the coefficient of variation of six replicate samples, was 15% in 1989-91, and 12% in
187 2012. In 2012, the accuracy of Hg measurements was verified using the ORMS-4 certified
188 reference material (CRM) from the National Research Council of Canada. Our measurements
189 were always within the confidence limits given for the CRM. No CRM was commercially
190 available at the time of MEDATLANTE-II and ALMOFRONT-I cruises, but accuracy was
191 checked using two independent Hg standard solutions. Easily-reducible Hg (often called
192 “reactive Hg”, HgR) was also systematically measured on board. The data, not reported here,
193 allowed the calculation of the mean HgR/HgT ratio, which was used to estimate the six
194 missing HgT values (see SI 1). The quality of the analytical measurements was ensured by
195 the use of the cleaning procedures for sampling and sample treatment that are recommended
196 by Gill and Fitzgerald (1985), Mason and Fitzgerald (1993) and more recently by the
197 GEOTRACES program, and by the rapidity of the onboard determinations after sampling. The

198 capability of the two laboratories (LOV-CNRS and IFREMER) for producing high-quality ultra-
199 trace measurements is shown by the results of their participation in most of the Hg
200 intercomparison exercises for the aquatic environments over the last 25 years (e.g., Cossa and
201 Courau, 1990; Lamborg et al., 2012).

202

203 **3. Results and Discussion**

204 ***3.1. Water masses and biogeochemical context***

205 West of Gibraltar, temperature and salinity distributions at Sta. 6A (1989) and Sta. 6B (2012)
206 are given in SI (Fig. S1a and b). The temperature *versus* salinity (T-S) graphs (Fig. 2) allow
207 the same water masses to be identified during the two cruises; the presence of these water
208 masses is well documented in this STG region (e.g., Pérez et al., 2018). Listing them from
209 surface to bottom: (i) the surface (mixed) layer, (ii) the North East Atlantic Central Water
210 (NEACW), (iii) the North East Atlantic Deep Water (NEADW) and (iv), at the bottom, the
211 Lower Deep Water (LDW). The NEACW in the STG is composed of different mode waters
212 including Mediterranean Water (MW) and Subpolar Mode Waters (SPMW), which both are
213 clearly identified on the T-S graph in Figure 2 by high and low salinities, respectively
214 (McCartney, 1992; Tsuchiya et al., 1992). The presence of MW is clearly identified by the
215 salinity maximum located between 800 and 1250 m (SI, Fig. S1). The salinity variations
216 along the Sta. 6A profiles testify to the presence of MW escaping the Strait of Gibraltar.
217 Salinity (herein S_p) is defined using the practical salinity scale from rosette sensor data.
218 Using salinity of 35.5 and 38.5 S_p for the Atlantic and Mediterranean end-members, the
219 proportions of MW at Sta. 6A varied around 25% in 1989 (MEDATLANTE-II cruise).
220 According to Yoon et al. (1996), who described zinc distribution from the same cruise, the
221 salinity maximum (36.37 S_p) corresponded to 32% of MW. At Sta. 6B occupied during the

222 FENICE cruise (2012), the MW proportion reached 28% at the salinity maximum. There, the
223 NEADW is underlain by the bottom layer constituted by LDW, which is a warmed Antarctic
224 Bottom Water (AABW) coming from the Southern Ocean (Fig. 2). This deepest water mass
225 contains very low chlorofluorocarbon (CFC's) concentrations, which attest for its pre-
226 industrial atmospheric imprint (Rhein et al., 2002) and a Hg inventory attributable to the Hg
227 solubility pump. During the MEDATLANTE-II cruise (1989), the soluble reactive phosphorus
228 (SRP) distribution varied from 0.01 to 1.23 $\mu\text{mol L}^{-1}$ between the surface and 2000 m. The
229 vertical profiles exhibited the typical pattern for this region with concentrations increasing
230 rapidly from surface to 500-600 m, then decreasing slightly. The MW was located between
231 800 and 1200 m (SI, Fig. S2a). At deeper depths, SRP concentrations continued to increase at
232 slower rates. During the FENICE cruise, at Sta. 6B, nutrient concentrations were not measured.
233 As a proxy for SRP, we use remineralized phosphate (P_{rem}) calculated from the Apparent
234 Oxygen Utilization (AOU) divided by a 141 Redfield ratio (Minster and Boulahdid, 1987),
235 suggesting P_{rem} varied from 0.49 to 1.22 $\mu\text{mol L}^{-1}$. The concentration range and shape of the
236 vertical profiles (SI, Fig. S2b) were similar during both the 1989 and 2012 cruises, suggesting
237 that the biogeochemical conditions affecting Hg remobilization remained relatively
238 unchanged during the 1989-2012 period.

239 In the Western Mediterranean Sea, the following water masses are from top to bottom:
240 the modified Atlantic waters (MAW), the Levantine Intermediate Water (LIW), the Winter
241 Intermediate Water (WIW), and the Western Mediterranean Deep Water (WMDW) (Millot et
242 al., 2006; Garcia-Lafuente et al., 2017). The LIW, identified by a salinity maximum, is
243 formed in the Eastern Mediterranean basin, while the WIW, identified by a temperature
244 minimum, is formed along the continental shelf of the North Western Mediterranean basin.
245 Finally, the WMDW is both the densest and coldest water present in the basin. The
246 hydrological structures found during the ALMOFRONT-I (1991) and FENICE (2012) cruises

247 were typical of the Alboran Sea (Tintoré et al., 1988; Béthoux et al., 2005). In addition, the
248 ALMOFRONT-I conditions were given in detail by Prieur and Sournia (1994), who described
249 the multiple-gyres and frontal structures. Station 4 (2012) was located in the Western Alboran
250 cyclonic gyre, whereas Stas. 7 (2012) and 36 (1991) were located eastward in the Almeria
251 cyclonic gyre, and Stas. 63 and 65 (1991) in the Cartagena anticyclonic eddy. Potential
252 temperature *versus* salinity (T_p -S) graphs are given in Fig. 3, and T_p and salinity profiles in
253 Fig. S3 (SI). The inflowing Atlantic water was located between 0 and 25 m depth with an
254 average $S < 37 S_p$, and MAW was identified down to 100 m ($S = 37$ - $38 S_p$). The WIW ($S =$
255 38.2 - $38.3 S_p$) was found below 125 m down to the maximum of salinity at around 400 m,
256 which characterized the LIW. The WMDW was located below 900 m depth ($S = 38.42 S_p$).
257 During the FENICE cruise, the T-S graph of Stas. 4 and 7 exhibited the same hydrological
258 structure with the presence of MAW, WIW-LIW, and WMDW. In addition, surface
259 temperatures of 18-25 °C showed the extension of summer surface stratification (FENICE
260 cruise) that was not observed in spring (ALMOFRONT-I cruise). In the Alboran Sea,
261 phosphorus concentrations varied from low values in surface waters to P_{rem} of $0.5 \mu\text{mol L}^{-1}$ in
262 1991. In 2012, P_{rem} also reached $0.6 \mu\text{mol L}^{-1}$ in deep waters. Vertical dissolved phosphorus
263 profiles are shown (Fig. S4, SI). The P_{rem} data obtained in 2012 (FENICE cruise) were
264 calculated from the AOU divided by a factor of 237, the specific Redfield ratio for the
265 Western Mediterranean due to the P limitation of this oceanic region (Béthoux et al., 2005).

266 **3.2. Mercury distributions**

267 West of Gibraltar, in the Eastern North Atlantic, HgT concentrations measured in 1989 (Sta.
268 6A) varied from 0.21 to 1.07 pmol L^{-1} (Fig. 4). They ranged from 0.21 to 0.75 pmol L^{-1} in the
269 surface layer, and increased from 0.21 at 40 m to $\sim 1 \text{ pmol L}^{-1}$ at 500 m within the SPMW,
270 characterized by low temperature and salinity, and by peaking phosphorus levels (Fig. S1 and
271 S2, SI). Below this depth, the profile showed a small Hg peak between 1000 and 1200 m.

272 This relative maximum corresponds to the water layer (open circles in Fig. 4) where high
273 salinity and low nutrients indicate the highest proportion of MW (Fig. SI, S1). Below 1200
274 m, the HgT levels were relatively less variable and ranged between 0.95 and 1.07 pmol L⁻¹ in
275 the NEADW and LDW. In comparison, HgT concentrations measured in 2012 (Sta. 6B)
276 varied within a similar range, from 0.19 to 0.95 pmol L⁻¹. However, the concentrations were
277 clearly lower in the NEACW (Fig. 4). The presence of MW at ~1000 m comes with a small
278 inflexion in the HgT profile (open circles in Fig. 4). At greater depths (>3000 m), HgT
279 concentrations, obtained in 1989 and 2012, were converging to a mean value of 0.96 ± 0.04
280 pmol L⁻¹ reached within the LDW. Since LDW results from the mixing of AABW with North
281 Atlantic Deep waters during its northward transit, its relatively high mean HgT concentration
282 is consistent with the elevated concentrations found recently (2014) in the lower NEADW
283 during the GEOTRACES GA-01 transect (1.04 ± 0.02 pmol L⁻¹ according to Cossa et al.,
284 2018a) and at the source of AABW in the Southern Ocean in 2008 (1.35 ± 0.31 pmol L⁻¹)
285 (Cossa et al., 2011). It can be surprising that, at depth as deep as 2500 m, HgT concentrations
286 may have changed in a 20-years period. West of Gibraltar, NEADW spread down to 3000 m (Fig.
287 4). According to García-Ibáñez (2015), the water mass present at 3000 m is composed of 50-60% of
288 LDW (called by these authors “lower-NEADW” or NEADWL) and similar proportions (20-25%) of
289 LSW (Labrador Sea water) and ISOW (Island Scotland Outflow water). With a ventilation age of
290 more than 150 years, NEADWL cannot contain recent anthropogenic Hg from the solubility pump.
291 Conversely, LSW and ISOW, which are younger than 20 years (Doney et al., 1997), may have
292 undergone changes in the Hg incorporation within the 1989-2012 period. Furthermore, in the layer of
293 NEADW between 3000 and 2500 m the proportion of NEADWL is decreasing to 40% and at 2000 m
294 it is less than 20%, whereas, parallelly, the proportion of the younger LSW is increasing up to 60%.
295 Thus, a HgT change down to 2500-3000 m, at this place of the Northeast Atlantic Ocean within the
296 1989-2012 period, is rational.

297 East of Gibraltar, in the Alboran Sea (Fig. 1), HgT concentrations measured in 1991
298 varied from 1.28 to 2.44 pmol L⁻¹ in the MAW, with an average of 1.71 pmol L⁻¹. They
299 reached values higher than 2 pmol L⁻¹ in the WIW, and averaged 1.42 and 1.32 pmol L⁻¹ in
300 the LIW and WMDW, respectively (Fig. 5). On the other hand, HgT concentrations measured
301 in 2012 were clearly lower for the same water masses (0.33 to 0.96 pmol L⁻¹). Interestingly
302 and in contrast to 1991, the lowest values in the subsurface waters were associated with the
303 MAW probably as results of photoreduction and evaporation of Hg volatile species, whereas
304 the highest were observed at depth (Fig. 5).

305 ***3.3. Time trends in Hg concentrations***

306 Simple calculations can be done to estimate the temporal decrease of HgT concentration from
307 direct comparison of the vertical profiles obtained in 1989, 1991 and 2012 (Figs. 4 and 5).
308 West of Gibraltar, the amplitude of the Hg decrease diminished with depth. It ranges from
309 ~50% in SPMW/NEACW to ~40% in MW/NEACW and ~35% in the upper NEADW. This
310 last estimate is consistently similar to the 30% decline of Hg mean concentration observed in
311 the core of LSW during the last 20 years (Cossa et al., 2018a). Below, in the aged LDW, no
312 HgT change seems to have occurred between 1989 and 2012. East of Gibraltar, the observed
313 decrease is ~30% in the herein sampled WMDW.

314 Another way to estimate the Hg decrease in the last 20 years that may reveal changes
315 in the biogeochemical context, is to look at changes in the Hg/nutrient ratios. Indeed, Hg is
316 thought to exhibit a nutrient-like behaviour in the North Atlantic Ocean (Cossa et al., 2004
317 and 2018a; Lamborg et al., 2014b; Bowman et al., 2015). This is confirmed by the
318 statistically significant correlations between Hg and SPR or P_{rem} concentrations in both the
319 1989 and 2012 cruises west of Gibraltar (R² = 0.94 and 0.92, respectively, Fig. 6a). The
320 regression coefficient calculated with 2012 data from Sta. 6B is 0.87 μmol_{Hg}/mol_P based on
321 an AOU/P_{rem} of 141 (Minster and Boulahdid, 1987), and it is 1.05 μmol_{Hg}/mol_P if AOU/P_{rem}

322 is 171 according to Lamborg et al. (2014b). This latter value is similar to that obtained for
323 oceanic water not suspected of containing anthropogenic Hg, namely 1.02 ± 0.03
324 $\mu\text{mol}_{\text{Hg}}/\text{mol}_{\text{P}}$ (Lamborg et al., 2014b). The regression slope obtained in 1989 was lower (0.57
325 $\mu\text{mol}_{\text{Hg}}/\text{mol}_{\text{P}}$ based on an $\text{AOU}/\text{P}_{\text{rem}}$ of 141, or $0.69 \mu\text{mol}_{\text{Hg}}/\text{mol}_{\text{P}}$ if $\text{AOU}/\text{P}_{\text{rem}}$ is 171)
326 reflecting Hg-enrichment in P-poor surface water (Fig. 6a). According to the Lamborg et al.
327 (2014b) model, this enrichment would be due to anthropogenic Hg since a “pristine
328 relationship” is characterized by the global relationship for the World Ocean of $\text{Hg}_{[\text{pmol L}^{-1}]} =$
329 $1.01 * \text{P}_{\text{rem}[\mu\text{mol L}^{-1}]} - 0.07$ (see discussion in the *Supplementary Information* section in Lamborg
330 et al.’s paper). The nutrient-like behavior of Hg means that a large fraction of surface Hg is
331 drawn down to the ocean interior by sinking particles, where it is released as a result of
332 organic matter microbiological remineralization, according to the well-known biological
333 pumping/regeneration process (Sigman and Haug, 2006). East of Gibraltar, during the FENICE
334 cruise in 2012, the Hg *versus* P_{rem} relationships were also statistically significant ($R^2 = 0.95$
335 and 0.76 at Stas 4 and 7, respectively, Fig. 6b). In contrast, during the ALMOFRONT-I cruise in
336 1991, the absence of a significant Hg *versus* SRP relationship (Fig. 6b) illustrated the fact
337 that the major Hg enrichment at Stas. 63-65 was especially elevated in surface waters (Fig.
338 5). Normalized to common P concentrations, the Hg concentration decrease between 1991
339 and 2012 in the east of Gibraltar ranges $\sim 38\%$ for WMDW (for $\text{P} = 0.6 \mu\text{mol L}^{-1}$). West of
340 Gibraltar, the P-normalized Hg decrease between 1989 and 2012 is $\sim 30\%$ at 1000 m (for $\text{P} =$
341 $1.2 \mu\text{mol L}^{-1}$) (i.e., in the MW/NEACW) increasing up to $>50\%$ in the subsurface water (i.e.,
342 upper SPMW/NEACW) (for $\text{P} = 0.6 \mu\text{mol L}^{-1}$).

343 It is interesting to note the contrasting situation which exists for deep waters east and
344 west of Gibraltar. In the Alboran Sea, the Hg decrease is 30-38% in ~ 20 years old WMDW
345 (Bethoux et al., 2005; Schneider et al., 2014), whereas, on the Atlantic side of Gibraltar
346 Strait, the HgT concentration did not vary in the LDW between 1989 and 2012 (Fig. 4). This

347 is entirely consistent with the pre-industrial age of these deepest oceanic waters. Furthermore,
348 the Hg decrease between 1989 and 2012 west of Gibraltar appears to be smaller for the oldest
349 waters (NEADW) than that for younger ones (SPMW/NEACW). This result is consistent
350 with the smaller decrease (30%) of the anthropogenic Hg fraction modeled in the deep waters
351 of the North Atlantic at 35°N compared to that modeled at shallower depths (70%) (e.g.,
352 OFFTRAC-GEOS-Chem model; Zhang et al., 2014b). A minor part of the temporal decline
353 in Hg concentrations in the intermediate waters of the North Atlantic between 1989 and 2012
354 might be attributed to the reduced efficiency of the biological pump, since the oceanic
355 primary production of North and Central Atlantic has slightly (-7%) decreased since the
356 early 1980s (Gregg et al., 2003). The dramatic drop of Hg concentrations actually observed in
357 intermediate waters likely reflects the reduction in Hg deposition over the North Atlantic
358 region over time (Soerensen et al., 2012; Weigelt et al., 2014). Indeed, this trend follows the
359 temporal decline in Hg emission inventories for the Eastern United States of America since
360 the mid-1990's years (Zhang et al., 2014b). Such decrease has already been observed in the
361 North Western Atlantic near Bermuda but in sub-surface waters (Mason et al., 2012;
362 Lamborg et al., 2014b). Additionally, recent Hg measurements performed in the water
363 column of the North Eastern Atlantic in 2010 (GA-03 section) and 2014 (GA-01 section)
364 (Fig. 4; Bowman et al., 2015; Cossa et al., 2018a) indicate, together with our dataset, that Hg
365 concentrations have been declining between 1989 (Sta. 6A), 2010 (e.g., 0.68-0.89 pmol L⁻¹ at
366 Sta. 5) and 2012 (Sta. 6B) in the core of NEADW. Conversely, no significant decrease is
367 observed between 2012 (Sta. 6B) and 2014 (Sta. 13), since Hg_T concentration ranges and
368 distribution at depth were similar at both years (Fig. 4).

369 In the Alboran Sea, sources of Hg are (i) Atlantic waters inflowing the Mediterranean
370 in surface, (ii) direct atmospheric deposition, and (iii) WIW, LIW and WMDW from the
371 Western Mediterranean at depth. As discussed above, the Atlantic surface waters, sampled

372 west of Gibraltar, show a decline in their Hg content (>50%) between 1989 and 2012. Thus,
373 the influx of Hg from the Atlantic toward the Mediterranean is weakening with time. In
374 addition, Alboran Sea waters are influenced by riverine metal sources (the mine-
375 contaminated Tinto-Odiel-Huelva riverine system) inflowing the Gulf of Cadiz (van Geen et
376 al., 1991). In the case of Hg, the concentrations were elevated in those rivers (up to 330 pmol
377 L⁻¹ in the Odiel River), and in the surface waters of the Gulf of Cadiz, the average dissolved
378 Hg concentration was 2.9 ± 0.9 pmol L⁻¹ in 1997-98 (Cossa et al., 2001). In 2012, during the
379 2012 FENICE cruise, dissolved Hg concentrations in the Gulf of Cadiz averaged only $0.55 \pm$
380 0.17 pmol L⁻¹ (Knoery, unpublished). This decrease in Hg content in the Gulf of Cadiz
381 surface waters may have contributed to the Hg decrease in the MAW entering the Alboran
382 Sea. The direct Hg atmospheric deposition on the Alboran Sea has not been estimated.
383 However, an atmospheric record of CO, O₃ and Hg across the Western Mediterranean and the
384 Northeastern Atlantic (April 2012) indicates an Hg peak in the troposphere at Gibraltar,
385 probably due to the densification of maritime traffic and industrialization at the Strait
386 (Maruszczak et al., unpublished, Fig. S5, SI). At depth, the Hg concentrations in WMDW
387 have been found to be enriched during the winter water convection occurring in the Gulf of
388 Lions and the adjacent gyre (Cossa et al., 2018b). The efficiency of the convection, which
389 governs the Hg export at depth and its further exportation to the adjacent Northeast Atlantic,
390 is variable from year to year, driven by the intensity of winter cooling of surface water
391 (Marty and Chiaverini, 2010; Heimbürger et al., 2013; Macias et al., 2018). Furthermore, the
392 Hg export to the Atlantic (i.e., the “Hg clearing rate” of the Mediterranean Sea) may have
393 increased since the vertical export flux capacity seems to have increased since 1999 (Marty
394 and Chiaverini, 2010).

395

396 **Conclusions**

397 Our work reveals that the decrease in atmospheric Hg concentrations, observed at the turn of
398 the century in northern mid-latitudes, has had a measurable impact on the Hg content of
399 oceanic waters. We showed that, using identical sampling and analytical techniques during
400 four oceanographic cruises on both sides of the Strait of Gibraltar, Hg concentrations have
401 significantly decreased between 1989 and 2012. West of Gibraltar, the Hg decrease ranges
402 from ~35% in the upper NEADW to ~50% in the NEACW. East of Gibraltar, the observed
403 decrease is ~30% in the WMDW. In contrast, no change was observed in the deepest waters
404 (>3000 m) whose ventilation age exceeds 150 years, i.e. waters formed prior the industrial
405 era. These results corroborate the predicted decreasing Hg concentration trends in North
406 Atlantic waters (e.g., Sunderland and Mason, 2007) as well as the expected decline in the
407 Mediterranean Sea (Radjar et al., 2007). Our results suggest that regulations to reduce
408 anthropogenic Hg emissions, starting with the 1970 US Clean Air Act to the more recent
409 2017 International Minamata Convention (UNEP, 2013), have had a positive effect on Hg
410 contamination in parts of the marine environment. Abated anthropogenic Hg emissions
411 decrease the Hg influx to the marine environment, its subsequent entrapment in the ocean's
412 interior, and its availability for the formation of the toxic MeHg which biomagnifies through
413 marine food webs. All other factors governing Hg methylation and bioaccumulation being
414 equal, our results suggest that Hg bioavailability to Northeastern Atlantic and Western
415 Mediterranean pelagic ecosystems, including edible fish species, is likely to have decreased
416 between the two decades straddling the new millennium. A declining-trend in Hg levels in
417 fish tissue in North American lakes over the period 1972-2016 has recently been
418 demonstrated (Grieb et al., 2019), but in many cases the temporal trends in aquatic biota do
419 not parallel changes in atmospheric concentrations and processes other than Hg
420 concentrations must control MeHg bioaccumulation (Wang et al., 2019). Hence, more

421 information must be gathered to elucidate these complex processes, especially in marine
422 environments.

423

424 **References**

425 Amos, H.M., Jacob, D.J., Streets, D.G., Sunderland, E.M., 2013. Legacy impacts of all-time
426 anthropogenic emissions on the global mercury cycle. *Global Biogeochem. Cy.* 27, 410–
427 421, doi:10.1002/gbc.20040.

428 Béthoux, J.-P., El Boukhary, M.S., Ruiz-Pino, D., Morin, P., Copin-Montégut, C., 2005.
429 Nutrient, Oxygen and Carbon Ratios, CO₂ Sequestration and Anthropogenic Forcing in
430 the Mediterranean Sea. In: A. Saliot ed. *The Mediterranean Sea. Hdb. Env. Chem. Vol.*
431 *5, Part K*, pp. 67–86, Springer Berlin / Heidelberg. doi:10.1007/b107144.

432 Bloom, N.S., Crecelius, E.A., 1983. Determination of Mercury in Seawater at Subnanogram
433 per Liter Levels. *Mar. Chem.* 14, 49-55.

434 Blum, J.D., Popp, B.N., Drazen, J.C., Choy, A., Johnson, M.W., 2013. Methylmercury
435 production below the mixed layer in the North Pacific Ocean. *Nature Geosci.* 6, 879–
436 884.

437 Bowman, K.L., Hammerschmidt, C.R., Lamborg, C.H., Swarr, G., 2015. Mercury in the
438 North Atlantic Ocean: The U.S. GEOTRACES zonal and meridional sections. *Deep-Sea*
439 *Res. II* 116, 251–261.

440 Broecker, W.S., 1979. A revised estimate for the radiocarbon age of the North Atlantic deep
441 water. *J. Geophys. Res.* 84, 3218–3226, doi.org/10.1029/JC084iC06p03218.

442 Carracedo Segade, L.I., Gilcoto, M., Mercier, H., Pérez, F.F., 2015. Quasi-synoptic transport,
443 budgets and water mass transformation in the Azores–Gibraltar Strait region during
444 summer 2009. *Progr. Oceanogr.* 130, 47–64.

445 Clarkson T.W., Magos L., 2006. The toxicology of mercury and its chemical compounds.
446 *Critical Review in Toxicology* 36, 609–662.

447 Cole, A.S., Steffen, A., 2010. Trends in long-term gaseous mercury observations in the Arctic
448 and effects of temperature and other atmospheric conditions. *Atmos. Chem. Phys.* 10,
449 4661–4672.

- 450 Cooke, C.A., Balcom, P.H., Biester, H., Wolfe, A.P., 2009. Over three millennia of mercury
451 pollution in the Peruvian Andes, PNAS 106, 8830–8834.
- 452 Cossa, D., Courau, P., 1990. An international intercomparison exercise for total mercury in
453 seawater. Appl. Organomet. Chem. 4, 49–54.
- 454 Cossa, D., Martin, J.M., K. Takayanagi, K., Sanjuan, J., 1997. The Distribution and Cycling
455 of Mercury in the Western Mediterranean. Deep-Sea Res. II 44, 721–740.
- 456 Cossa, D., Elbaz-Poulichet, F., Nieto, J.M., 2001. Mercury in the Tinto-Odiel Estuarine
457 System (Gulf of Cadiz, Spain): Sources and Dispersion. Aquat. Geochem. 7, 1–12.
- 458 Cossa, D., Cotté-Krief, M.H., Mason, R.P., Bretaudeau-Sanjuan, J., 2004. Total mercury in
459 the water column near the shelf edge of the European continental margin. Mar. Chem.
460 90, 21–29.
- 461 Cossa, D., Averty, B., N. Pirrone, N., 2009. The origin of methylmercury in the open
462 Mediterranean water column. Limnol. Oceanogr. 54, 837–844.
- 463 Cossa, D., Heimbürger, L-E., Lannuzel, D., Rintoul, S.R., Butler, E.C.V., Bowie, A.R.,
464 Averty, B., Watson, R.J., Remenyi T., 2011. Mercury in the Southern Ocean. Geochim.
465 Cosmochim. Acta 75, 4037–4052.
- 466 Cossa, D., X. Durrieu de Madron, J. Schäfer, L. Lanceleur, S. Guédron, R. Buscail, B.
467 Thomas, J.-J. Naudin. 2017. The open sea as the main source of methylmercury in the
468 water column of the Gulf of Lions (Northwestern Mediterranean margin). Geochim.
469 Cosmochim. Acta 199, 212-231.
- 470 Cossa, D., Heimbürger, L.E., Pérez, F.F., García-Ibáñez, M.I., Sonke, J.E., Planquette, H.,
471 Lherminier, P., Boutorh, J., Cheize, M., Menzel, J.L. Barraqueta, J.L., Shelley, R.,
472 Sarthou, G., 2018a. Mercury distribution and transport in the North Atlantic Ocean along
473 the GEOTRACES-GA01 transect. Biogeosciences 15, 1–15.
- 474 Cossa, D., Durrieu de Madron, X., Schäfer, J., Guédron, S., Maruszczak, N., Castelle, S.,
475 Naudin, J.-J., 2018b. Sources and exchanges of mercury in the waters of the
476 Northwestern Mediterranean margin. Progr. Oceanogr. 163, 172–183,
477 doi.org/10.1016/j.pocean.2017.05.002.
- 478 Cunningham, S.A., 2000. Circulation and volume flux of the North Atlantic using synoptic
479 hydrographic data in a Bernoulli inverse. J. Mar. Res. 58, 1, 1–35.

480 Courau, P., 1983. Dosage du mercure minéral dissous. Chap. XIX, p. 227-249. In: Manuel
481 des Analyses Chimiques en Milieu Marin. Aminot, A., Chaussepied, M. eds. CNEXO
482 BNDO/ Documentation, Brest (France), ISBN 2-902721-10-2, 395 pp.

483 de Simone, F., Gencarelli, N., Hedgecock, I.M., Pirrone, N., 2016. A Modeling Comparison
484 of Mercury Deposition from Current Anthropogenic Mercury Emission Inventories.
485 Environ. Sci. Technol. 50, 5154–5162, doi:10.1021/acs.est.6b00691.

486 Doney, S.C., Jenkins, W.J., Bullister, J.L., 1997. A comparison of ocean tracer dating
487 techniques on a meridional section in the eastern North Atlantic. Deep-Sea Res. I 44,
488 603-626.

489 Driscoll, C.T., Mason, R.P., H.M., Jacob, D.J., Pirrone, N., 2013. Mercury as a Global
490 Pollutant: Sources, Pathways, and Effects. Environ. Sci. Technol. 47, 4967–4983,
491 doi:10.1021/es305071v.

492 Elbaz-Poulichet, F., Dezileau, L., Freydier, R., Cossa, D., Sabatier, P., 2011. A 3500-year
493 record of Hg and Pb contamination in a Mediterranean sedimentary archive (the Pierre
494 Blanche Lagoon, France), Environ. Sci. Technol. 45, 8642–8647.

495 EPA (Environmental Protection Agency, US). 2002. Method 1631, Revision E: Mercury in
496 water by oxidation, purge and trap, and cold vapor atomic fluorescence spectrometry,
497 EPA-821-R-02-019, water.epa.gov/scitech/methods/cwa/metals/mercury.

498 Fitzgerald, W.F., Lamborg, C.H., 2003. Geochemistry of Mercury in the Environment. In:
499 Treatise on Geochemistry, K. Turekian and H. Holland eds. Vol. 9, B.S. Lollar ed.,
500 Chap. 4. ISBN 0-08-044344-3. Elsevier, pp.107–148.

501 Fitzgerald, W.F., Lamborg, C.H., Hammerschmidt, C.R., 2007. Marine Biogeochemical
502 Cycling of Mercury. Chem. Rev. 107, 641–62, doi:10.1021/cr050353m.

503 García-Ibáñez, M.I., Pardo, P.C., Carracedo, L.I., Mercier, E., Lherminier, P., Ríos, A.F.,
504 Pérez, F.F., 2015. Structure, transports and transformations of the water masses in the
505 Atlantic Subpolar Gyre. Progr. Oceanogr., 135, 18-35,
506 dx.doi.org/10.1016/j.pocean.2015.03.009.

507 García-Lafuente, J., Naranjo, C., Sammartino, S., Sánchez-Garrido, J.C., Delgado, J., 2017.
508 The Mediterranean outflow in the Strait of Gibraltar and its connection with upstream
509 conditions in the Alborán Sea. Ocean Sci. 13, 195–207, doi:10.5194/os-13-195-2017.

510 Gencarelli, C.N., De Simone, F., Hedgecock, I.M., et al., 2015. European
511 and Mediterranean mercury modelling: Local and long-range contributions to the
512 deposition flux. *Atmos. Environ.* 117, 162–168.

513 Gill, G.A., Fitzgerald, W.F., 1985. Mercury sampling of open ocean waters at the picomolar
514 level, *Deep-Sea Res. A* 32, 287–297, doi.org/10.1016/0198-0149(85)90080-9.

515 Gregg, W.W., Conkright, M.E., Ginoux, P., O'Reilly, J.E., Casey, N.W., 2003. Ocean
516 primary production and climate: Global decadal changes. *Geophys. Res. Lett.* 30, 15,
517 1809, doi:10.1029/2003GL016889.

518 Grieb, T.M., Fisher, N.S., Karimi, R., Levin, L., 2019. An assessment of temporal trends in
519 mercury concentrations in fish. *Ecotoxicology*, doi.org/10.1007/s10646-019-02112-3.

520 Heimbürger, L.E., Lavigne, H., Migon, C., d'Ortenzio, F., Estournel, C., Coppola, L.,
521 Miquel, J.-C., 2013. Temporal variability of vertical export flux at the DYFAMED time-
522 series station (Northwestern Mediterranean Sea). *Progr. Oceanogr.* 119, 59–67.

523 Hollweg, T.A., Gilmour, C.C., Mason, R.P., 2010. Mercury and methylmercury cycling in
524 sediments of the mid-Atlantic continental shelf and slope. *Limnol. Oceanogr.* 55, 2703–
525 2722.

526 Jensen, S., Jernelöv, A., 1969. Biological methylation of mercury in aquatic organisms.
527 *Nature* 223, 753–754.

528 Lamborg, C.H., Hammerschmidt, C.R., Gill, G.A., Mason, R.P., Gichuki, S., 2012. An
529 intercomparison of procedures for the determination of total mercury in seawater and
530 recommendations regarding mercury speciation during GEOTRACES cruises. *Limnol.*
531 *Oceanogr. Meth.* 10, 90–100, doi:10.4319/lom.2012.10.90.

532 Lamborg, C., Bowman, K., Hammerschmidt, C., Gilmour, C., Munson, K., Selin, N., Tseng,
533 C.-M., 2014a. Mercury in the anthropocene ocean. *Oceanography* 27, 76–87,
534 doi.org/1.5670/oceanog.2014.11.

535 Lamborg, C.H., Hammerschmidt, C.R., Bowman, K.L., Swarr, G.J., Munson, K.M.,
536 Ohnemus, D.C., Lam, P.J., Heimbürger, L.E., Rijkenberg, M.J.A., Saito, M.A., 2014b. A
537 global ocean inventory of anthropogenic mercury based on water column measurements.
538 *Nature* 512, 65–68.

539 Lamborg, C.H., Hammerschmidt, C.R., Bowman, K.L., 2016. An examination of the role of
540 particles in oceanic mercury cycling. *Phil. Trans. R. Soc. A* 374: 20150297.
541 <http://dx.doi.org/10.1098/rsta.2015.0297>

542 Macias, D., Garcia-Gorriz, E., Stips, A., 2018. Deep winter convection and phytoplankton
543 dynamics in the NW Mediterranean Sea under present climate and future (horizon 2030)
544 scenarios. *Sci. Rep.* 8, 6626. doi:10.1038/s41598-018-24965-0.

545 Mao, H., Talbot, R., 2012. Speciated mercury at marine, coastal, and inland sites in New
546 England – Part 1: Temporal variability, *Atmos. Chem. Phys.* 12, 5099-5112,
547 <https://doi.org/10.5194/acp-12-5099-2012>.

548 Marty, J.C., Chiavérini, J., 2010. Hydrological changes in the Ligurian Sea (NW
549 Mediterranean, DYFAMED site) during 1995–2007 and biogeochemical consequences.
550 *Biogeosciences* 7, 2117–2128.

551 Mason, R.P., Fitzgerald, W.F., 1990. Alkylmercury species in the Equatorial Pacific. *Nature*
552 347, 457–459.

553 Mason, R.P., Fitzgerald, W.F., 1993. The distribution and biogeochemistry cycling of
554 mercury in the Equatorial Pacific Ocean. *Deep-Sea Res. I* 40, 1897–1924.

555 Mason, R.P., Choi, A.L., Fitzgerald, W.F., Hammerschmidt, C.R., Lamborg, C.H.,
556 Soerensen, A.L. Sunderland, E.M., 2012. Mercury biogeochemical cycling in the ocean
557 and policy implications. *Environ. Res.* 119, 101–117.

558 Mason, R.P., Hammerschmidt, C.R., Lamborg, C.H., Bowman, K.L., Swarr, G.J., Shelley,
559 R.U., 2017. The air-sea exchange of mercury in the low latitude Pacific and Atlantic
560 Oceans. *Deep-Sea Res. I* 122, 17–28, doi.org/10.1016/j.dsr.2017.01.015.

561 McCartney, M.S., 1992. Recirculating components to the deep boundary current of the
562 northern North Atlantic. *Prog. Oceanogr.* 29, 283– 383.

563 Millot, C., Candela, J., Fuda, J.-L., Tber, Y. 2006. Large warming and salinification of the
564 Mediterranean outflow due to changes in its composition. *Deep-Sea Res. I* 53, 656–666,
565 doi:10.1016/j.dsr.2005.12.017.

566 Minster, J.-F., Boulahdid, M., 1987. Redfield ratios along isopycnal surfaces – a
567 complementary study. *Deep-Sea Res. I* 34, 1981–2003.

568 Monperrus, M., Tessier, E., Amouroux, D., Leynaert, A., Huonnic, P., Donard, O.F.X., 2007.
569 Mercury methylation, demethylation and reduction rates in coastal and marine surface
570 waters of the Mediterranean Sea. *Mar. Chem.* 10, 49–63.

571 Muntean, M, Janssens-Maenhout, G., Song, S., Selin, N.E., Olivier, J.G.J., Guizzardi, D.
572 Mass, R., Dentener, F., 2014. Trend analysis from 1970 to 2008 and model evaluation of
573 EDGARv4 global gridded anthropogenic mercury emissions. *Sci. Total Environ.* 494-
574 495, 337–350. <https://doi.org/10.1016/j.scitotenv.2014.06.014>.

575 Outridge, P.M., Mason, R.P., Wang, F., Guerrero, S., Heimbürger, L-E., 2018. Updated
576 global and oceanic mercury budgets for the United Nations Global Mercury Assessment
577 2018. *Environ. Sci. Technol.* 52, 11466-11477, doi:10.1021/acs.est.8b01246.

578 Parks, J.M., Johs, A., Podar, M., Bridou, R., Hurt, R.A., Smith, S. D., Tomanicek, S.J., Qian
579 Y., Brown, S.D., Brandt, C.C., Palumbo, A.V., Smith, J.C., Wall, J.D., Elias, D.A.,
580 Liang, L., 2013. The genetic basis for bacterial mercury methylation. *Science* 339, 1332–
581 1335.

582 Pérez, F.F., Fontela, M., García-Ibáñez, M.I., Mercier, H., Velo, A., Lherminier, P.,
583 Zunino, P., de la Paz, M., Alonso-Pérez, F., Guallart, E.F., Padin, X.A., 2018.
584 Meridional overturning circulation conveys fast acidification to the deep Atlantic
585 Ocean. *Nature* 554, 515–518, doi:10.1038/nature2549.

586 Pirrone, N., Cinnirella, S., Feng, X., Finkelman, R.B., Friedli, H.R., Leaner, J., Mason, R.P.,
587 Mukherjee, A.B., Stracher, G.B., Streets, D.G., Telmer, K., 2010. Global mercury
588 emissions to the atmosphere from anthropogenic and natural sources. *Atmos. Chem. and*
589 *Phys.* 10, 5951–5964.

590 Prestbo, E.M., Gay, D.A., 2009. Wet deposition of mercury in the US and Canada, 1996-
591 2005: Results and analysis of the NADP mercury deposition network (MDN). *Atmos.*
592 *Environ.* 43, 4223–4233.

593 Prieur, L., Sournia, A., 1994. “Almofront-1” (April–May 1991): an interdisciplinary study of
594 the Almeria-Oran geostrophic front, SW Mediterranean Sea. *J. Mar. Syst.* 5, 187 –203.

595 Rajar, R., Cetina, M., Horvat, M., Zagar, D., 2007. Mass balance of mercury in the
596 Mediterranean Sea. *Mar. Chem.* 107, 89–102.

597 Rhein, M., Fisher, J., Smethie, W.M., Smythe-Wright, D., Weiss, R.F., Mertens, C., Min, D.-
598 H., Fleischmann, U., Putzka, A., 2002. Labrador Sea water: Pathways, CFC Inventory,
599 and Formation Rates. *J. Phys. Oceanogr.* 32, 648–665.

600 Schneider, A., Tanhua, T., Roether, W., Steinfeldt, R., 2014. Changes in ventilation of the
601 Mediterranean Sea during the past 25 year. *Ocean Sci.* 10, 1–16.

602 Semeniuk, K., and A. Dastoor. 2017. Development of a global ocean mercury model with a
603 methylation cycle: Outstanding issues, *Global Biogeochem. Cy.* 31, 400–433,
604 doi:10.1002/2016GB005452.

605 Sigman, D.M., Haug, G.H., 2006. The biological pump in the past. In: *Treatise on*
606 *Geochemistry*, K. Turekian and H. Holland eds. Vol. 6, H. Elderfield ed., pp. 625. ISBN
607 0-08-043751-6. Elsevier, 2003., p.491-528.

608 Slemr, F., Brunke, E.G., Ebinghaus, R., Kuss, J., 2011. Worldwide trend of atmospheric
609 mercury since 1995. *Atmos. Chem. Phys.* 11, 4779–4787.

610 Soerensen, A.L., Sunderland, E.M., Holmes, C.D., Skov, H., Christensen, J.H., Jacob, D.J.,
611 Strode, S., Mason, R.P., 2010. An Improved Global Model for Air-Sea Exchange of
612 Mercury: High Concentrations over the North Atlantic. *Environ. Sci. Technol.* 44, 8574-
613 8580.

614 Soerensen, A.L., Jacob, D.J., Streets, D.G., Witt, M.L.I., Ebinghaus, R., Mason, R.P.,
615 Andersson, M., Sunderland, E.M., 2012. Multi-decadal decline of mercury in the North
616 Atlantic atmosphere explained by changing subsurface seawater concentrations. *Geophys.*
617 *Res. Lett.* 39, 6 pages, L21810, doi:10.1029/2012GL053736.

618 Soerensen, A.L., Jacob, D.J., Schartup, A.T., Fisher, J.A., Lehnher, I., St. Louis, V.L.,
619 Heimbürger, L.E., Sonke, J.E., Krabbenhoft, D.P., Sunderland, E.M., 2016. A Mass
620 Budget for Mercury and Methylmercury in the Arctic Ocean. *Global Biogeochem. Cy.*
621 30 (4) (April): 560–575. Portico. doi:10.1002/2015gb005280.

622 Sonke, J.E., Heimbürger, L.-E., Dommergue, A., 2013. Mercury biogeochemistry: paradigm
623 shifts, outstanding issues and research needs. *CR Geosci.* 345, 213–222.

624 Sprovieri, F., Pirrone, N., Ebinghaus, R., Kock, H., Dommergue, A., 2010. A review of
625 worldwide atmospheric mercury measurements. *Atmos. Chem. Phys.* 10, 8245–8265.

626 Streets, D.G., Zhang, Q., Wu, Y., 2009. Projections of global mercury emissions in 2050.
627 *Environ. Sci. Technol.* 43, 2983–2988.

- 628 Sunderland, E.M., Mason, R.P., 2007. Human impacts on open ocean mercury
629 concentrations. *Global Biogeochem. Cy.* 21, GB4022, 1–15.
630 <https://doi.org/10.1029/2006GB002876>.
- 631 Tintoré, J., La Violette, P.E., Blade, I., Cruzado, A., 1988. A Study of an Intense Density
632 Front in the Eastern Alboran Sea: The Almeria-Oran Front. *J. Phys. Oceanogr.* 18, 1384–
633 1397.
- 634 Tsuchiya, M., Talley, L.D., McCartney, M.S., 1992. An eastern Atlantic section from Iceland
635 southward across the equator. *Deep-Sea Res. Part A* 39, 1885–1917.
- 636 UNEP, 2013. *Global Mercury Assessment 2013: Sources, Emissions, Releases*
637 *and Environmental Transport*. UNEP Chemicals Branch, Geneva, Switzerland.
638 <http://wedocs.unep.org/handle/20.500.11822/7984>.
- 639 Van Geen, A., Boyle E.A., Moore, W.S., 1991. Trace metal enrichments in waters of the Gulf
640 of Cádiz, Spain. *Geochim. Cosmochim. Acta* 55, 2173–2191.
- 641 Wang, F., Outridge, P.M., Feng, X., Meng, B., Heimbürger-Boavida, L.E., Mason, R.P.,
642 2019. How closely do mercury trends in fish and other aquatic wildlife track those in the
643 atmosphere? – Implications for evaluating the effectiveness of the Minamata
644 Convention. *Sci. Total Environ.* 674, 58-70.
- 645 Weigelt, A., Ebinghaus, R., Manning, A.J., Derwent, R.G., Simmonds, P.G., Spain, T.G.,
646 Jennings, S.G., Slemr, F., 2014. Analysis and Interpretation of 18 years of mercury
647 observations since 1996 at Mace Head, Ireland. *Atmos. Environ.* 100, 85–93.
- 648 Yoon, Y.-Y., Han, M.-H., Lee, J.-S., 1996. Distribution of Zn Concentrations in the Western
649 Mediterranean Sea and its Influence on the North East Atlantic Ocean. *Environ. Engin.*
650 *Res.* 2, 41–49.
- 651 Zhang, Y., Jaeglé, L., Thompson, L.A., 2014a. Natural biogeochemical cycle of mercury in a
652 global three-dimensional ocean tracer model, *Global Biogeochem. Cy.* 28, 553–570,
653 [doi:10.1002/2014GB004814](https://doi.org/10.1002/2014GB004814).
- 654 Zhang, Y., Jaeglé, L., Thompson, L.A., Streets, D.G., 2014b. Six centuries of changing
655 oceanic mercury, *Global Biogeochem. Cy.* 28, 1251–1261, [doi:10.1002/2014GB004939](https://doi.org/10.1002/2014GB004939).
- 656 Zhang, Y., Jacob, D.J., Horowitz, H.M., Chen, L., Amos, H.M., Krabbenhoft, D.P., Slemr, F.,
657 St. Louis, V.L., Sunderland, E.M., 2016. Observed decrease in atmospheric mercury

658 explained by global decline in anthropogenic emissions. PNAS 113, 526–531,
659 www.pnas.org/cgi/doi/10.1073/pnas.1516312113.

660
661

662 **Abbreviations**

663 AABW: Antarctic Bottom Water

664 AOU: Apparent oxygen utilization

665 BrCl: Bromine monochloride

666 CFC's: Chlorofluorocarbons

667 CO: Carbon monoxide

668 CRM: Certified reference material

669 FEP: Fluorinated ethylene propylene

670 GEOTRACES: An international study of the marine biogeochemical cycles of trace elements
671 and their isotopes (www.geotraces.org)

672 Hg: Mercury

673 Hg⁰: Elemental mercury

674 HgR: Reactive or easily reduced mercury

675 HgT: Total mercury

676 HgTUNF: Total mercury in unfiltered samples

677 HgTF: Total mercury in filtered samples

678 LDW: Lower Deep Water

679 LIW: Levantine Intermediate Water

680 LSW: Labrador Sea Water

681 MeHg: Methyl mercury

682 MAW: Modified Atlantic Water

683 MW: Mediterranean Water

684 NEACW: North East Atlantic Central Water

685 NEADW: North East Atlantic Deep Water

686 O₃: Ozone
687 OFFTRAC: University of Washington three-dimensional offline ocean tracer model.
688 ORMS-4: Certified reference material (River water spiked with inorganic mercury).
689 P: Phosphorus
690 P_{rem}: Remineralized phosphorus
691 SnCl₂: Tin chloride
692 SPMW: Subpolar Mode Water
693 SRP: Soluble reactive phosphorus
694 US-EPA: Environmental Protection Agency of the United States of America
695 WIW: Winter Intermediate Water
696 WMDW: Western Mediterranean Deep Water

697

698 **Figure captions**

699 **Figure 1.** Sampling locations within the North-eastern Atlantic Ocean and Western
700 Mediterranean during the MEDALANTE-II, ALMOFRONT-I and FENICE cruises. Sta. 6A on
701 September 5, 1989 (35.6732°N; 13.1588°W, bottom depth 4460 m); Sta. 6B on August 18,
702 2012 (35.5137°N; 09.1532°W, bottom depth 3610 m); Sta. 36 on April 30, 1991 (36.2231°N;
703 2.5336°W, bottom 987 m); Sta. 63 on May 3, 1991 (36.2183°N; 1.0733°W, bottom 2601 m);
704 Sta. 65 on 3 May, 1991 (36.3169°N; 0.5831°W, 2657 m); Sta. 4 on August 16, 2012
705 (36.4971°N; 4.0356°W, bottom 680 m) ; Sta. 7 on August 15, 2012 (35.9039°N; 2.6943°W,
706 bottom 990 m). In addition, Sta. 5 (31°N; 22°W, bottom 5175 m) and Sta. 13 (41.3830°N;
707 13.8877°W, bottom 5350 m) were occupied during the GEOTRACES-GA03 (August 2010) and
708 GA-01 (June 23, 2014), respectively. Arrows indicate main patterns of oceanic circulation:
709 Atlantic surface waters entering the Mediterranean Sea through the Gibraltar Strait, Modified
710 Atlantic Water (MAW) at the surface in the Alboran Sea, and at depth: Levantine
711 Intermediate Water (LIW), Western Mediterranean Deep Water (WMDW).

712 **Figure 2.** Salinity-Temperature graphs in the water column West of Gibraltar at Stas. 6A and
713 6B during the MEDATLANTE-II and FENICE cruises. NEACW: North East Atlantic Central
714 Water; NEADW: North East Atlantic Deep Water; LDW: Lower Deep Water; SPMWs:

715 Subpolar Mode Waters; MW: Mediterranean Water; LSW: Labrador Sea Water; ISOW:
716 Island Scotland Outflow Water; AABW: Antarctic Bottom Water.

717 **Figure 3.** Salinity-Temperature graphs in the water column East of Gibraltar at Stas. 63, 65, 4
718 and 7 during the ALMOFRONT-I and FENICE cruises. Modified Atlantic Water; WIW: Winter
719 Intermediate Water; LIW: Levantine Intermediate Water; WMDW: Western Mediterranean
720 Deep Water.

721 **Figure 4.** Concentration profiles of total Hg (HgT) West of Gibraltar at Sta. 6A (FENICE
722 cruise), Sta. 6B (MEDATLANTE-II cruise), Sta. 5 (31°N; 22°W, GEOTRACES GA-03 cruise),
723 Sta. 13 (41°23'N; 13°53'W, GEOTRACES GA-01 cruise). Open marks correspond to salinity
724 maxima due to the presence of the maximum proportion ($\leq 25\%$) of Mediterranean waters
725 (MW) along with the profile. NEACW: North East Atlantic Central Water; NEADW: North
726 East Atlantic Deep Water; LDW: Lower Deep Water.

727 **Figure 5.** Concentration profiles of total Hg (HgT) east of Gibraltar at Stas. 36, 63 and 65
728 (ALMOFRONT-I cruise), and Stas. 4 and 7 (FENICE cruise). MAW: Modified Atlantic Water;
729 WIW: Winter Intermediate Water; LIW: Levantine Intermediate Water; WMDW: Western
730 Mediterranean Deep Water.

731 **Figure 6.** Relationships between concentrations of total Hg (HgT) and soluble reactive
732 phosphorus (SRP) or remineralized phosphorus (P_{rem}). (a) West of Gibraltar at Stas. 6A and
733 6B, (b) east of Gibraltar at Stas. 4 and 7.

1
2
3
4
5
6
7
8
9
10
11
12
13
14
15
16
17
18
19
20
21
22
23
24
25
26
27
28
29
30
31
32
33
34
35
36
37
38
39
40
41
42
43
44
45
46
47
48
49
50
51
52
53
54
55
56
57
58
59
60
61
62
63
64
65

1 **Oceanic mercury concentrations on both sides of the Strait of Gibraltar**
2
3 **decreased between 1989 and 2012**

3

4 **Acknowledgments:** This research has been funded by the “Programme Flux Océaniques” conducted by CNRS
5 as the French part of the international JGOFS, and the Global Mercury Observation System (GMOS, N°265113
6 European Union project), and the European Research Council (ERC-2010-StG-20091028). Thanks are due to P.
7 Morin and Y. Le Merrer for providing nutrient data, K. Bowman for providing the HgT values at Sta. 5
8 (GEOTRACES, GA-03 transect), and M. Vautour and A. Mucci for English editing.

Figure

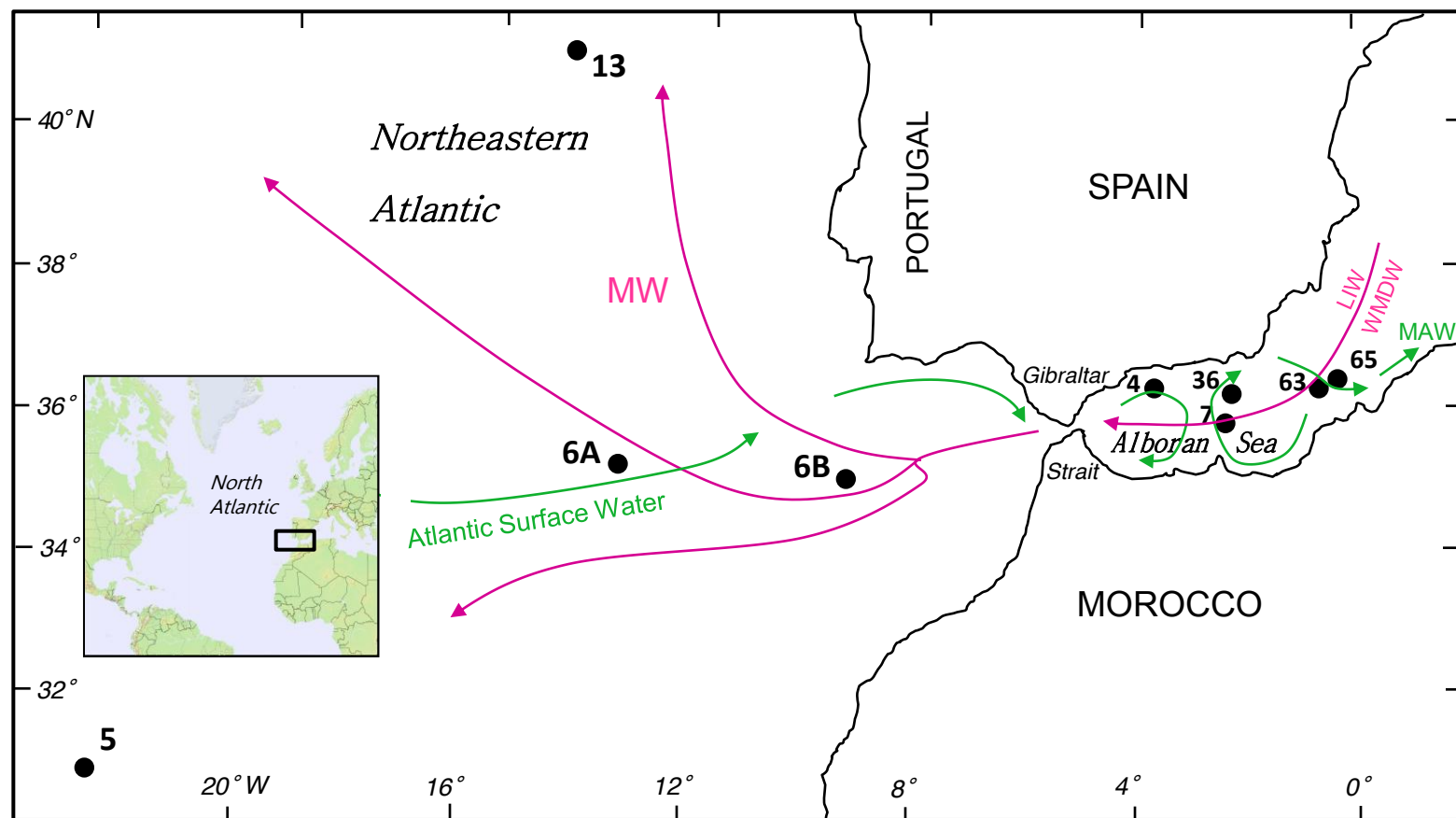


Fig. 1

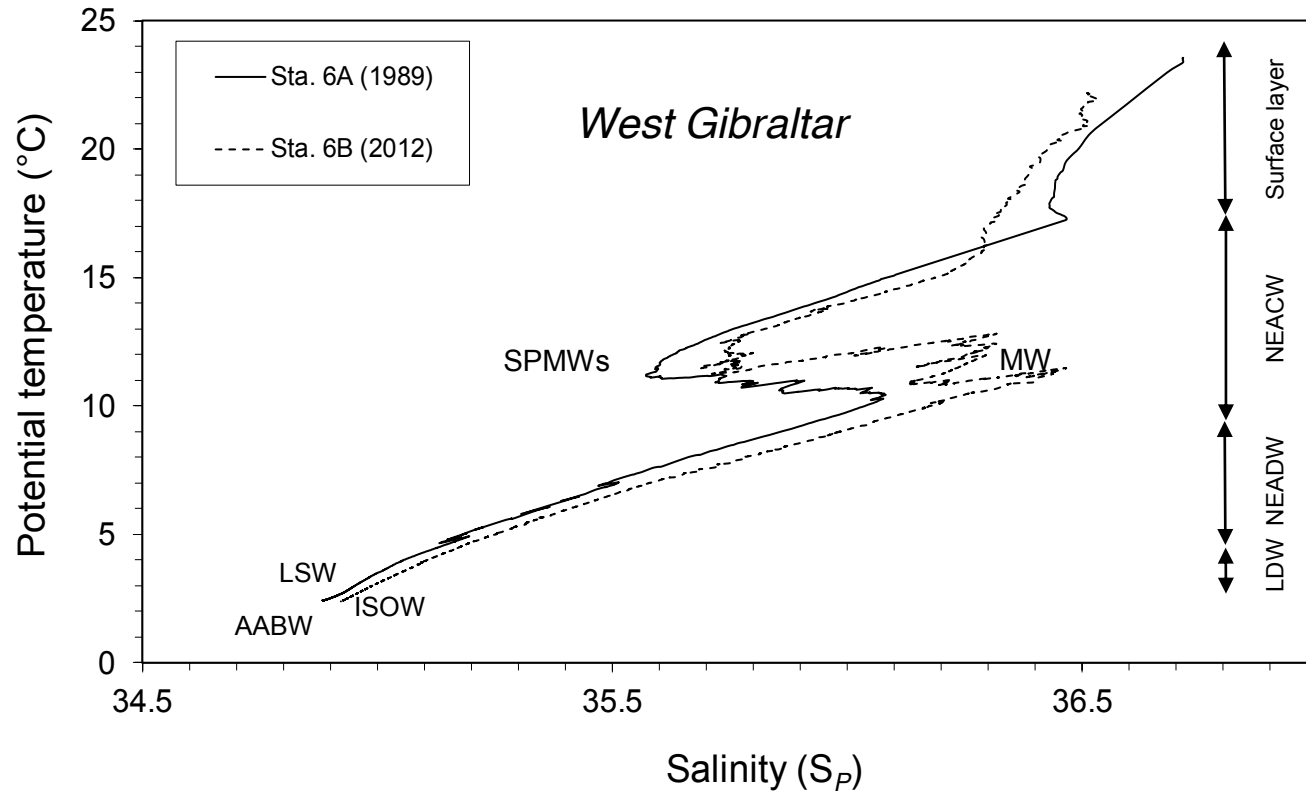


Fig. 2

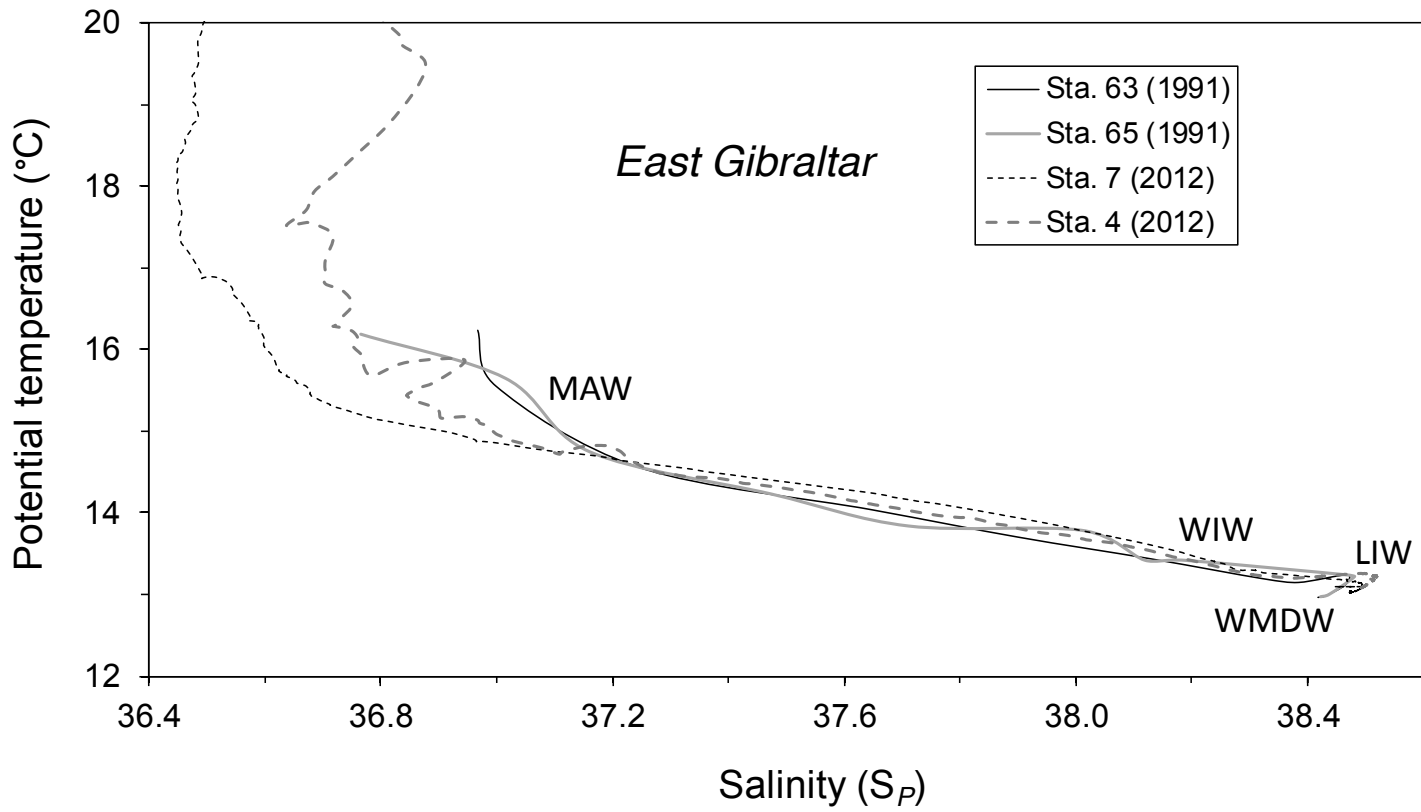


Fig. 3

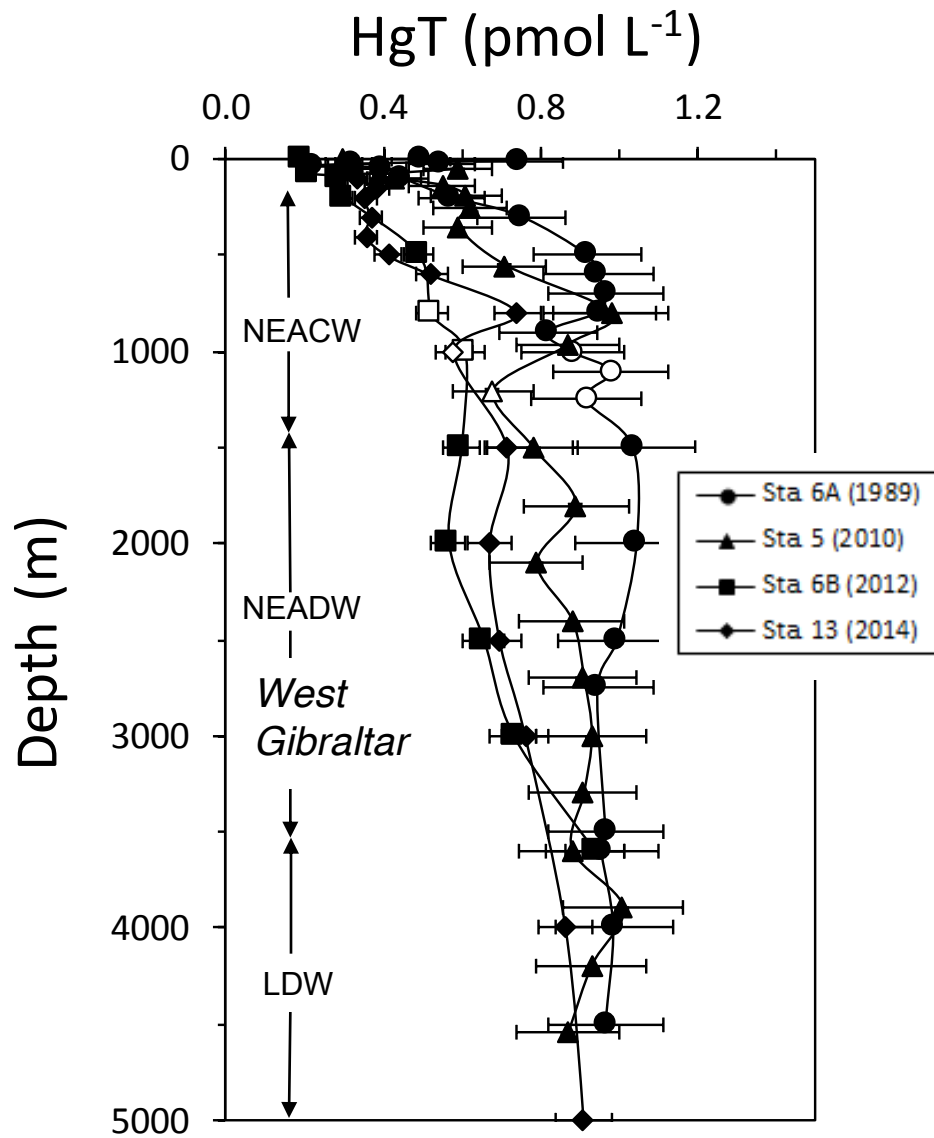


Fig. 4

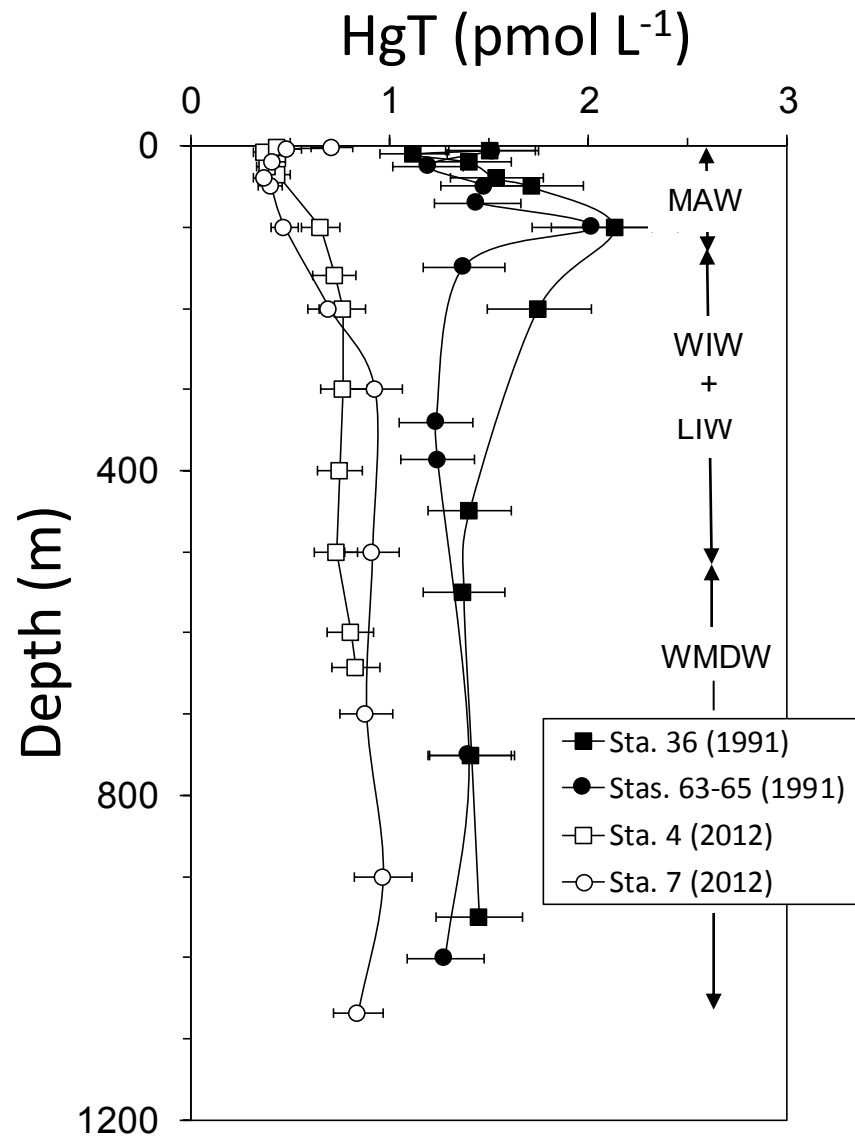


Fig. 5

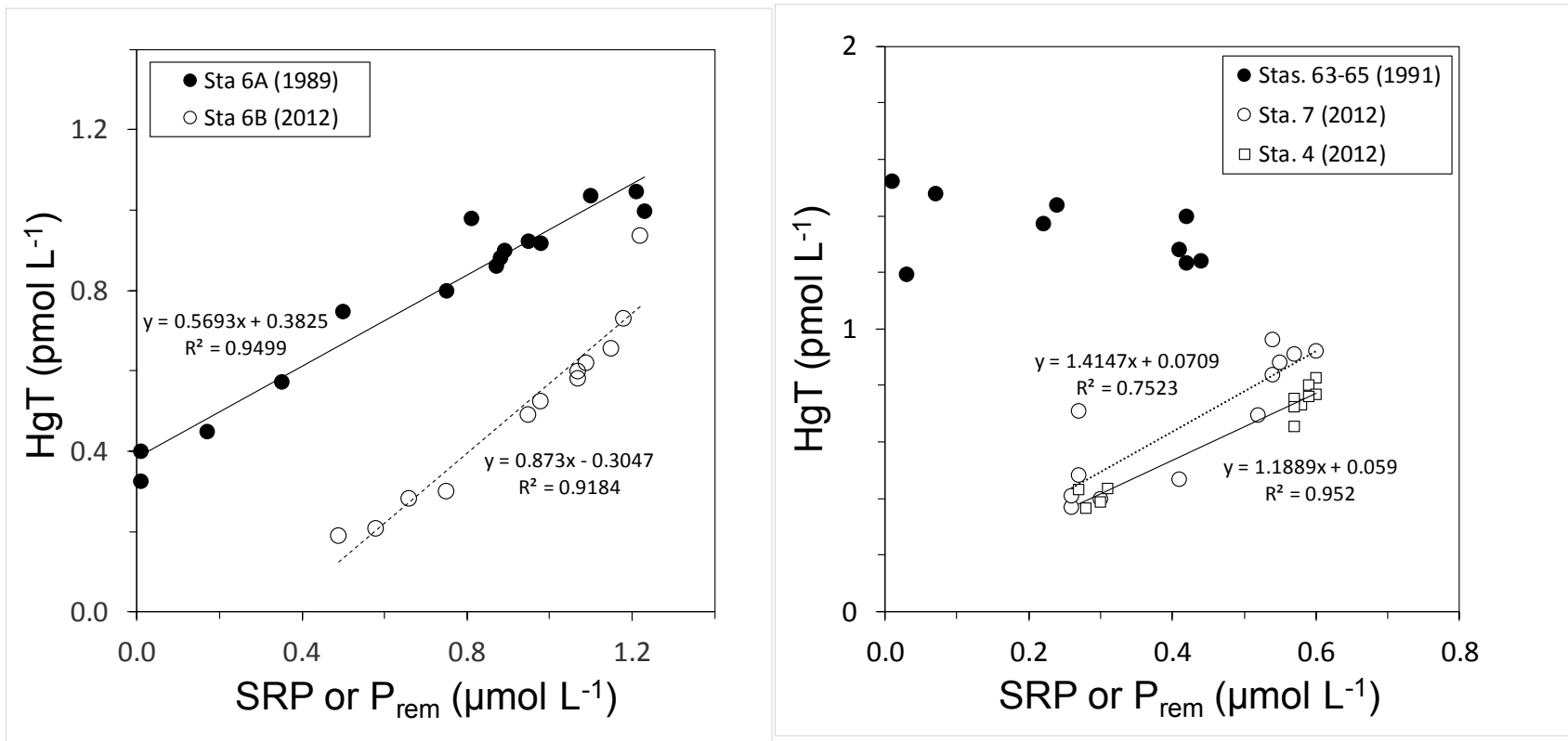
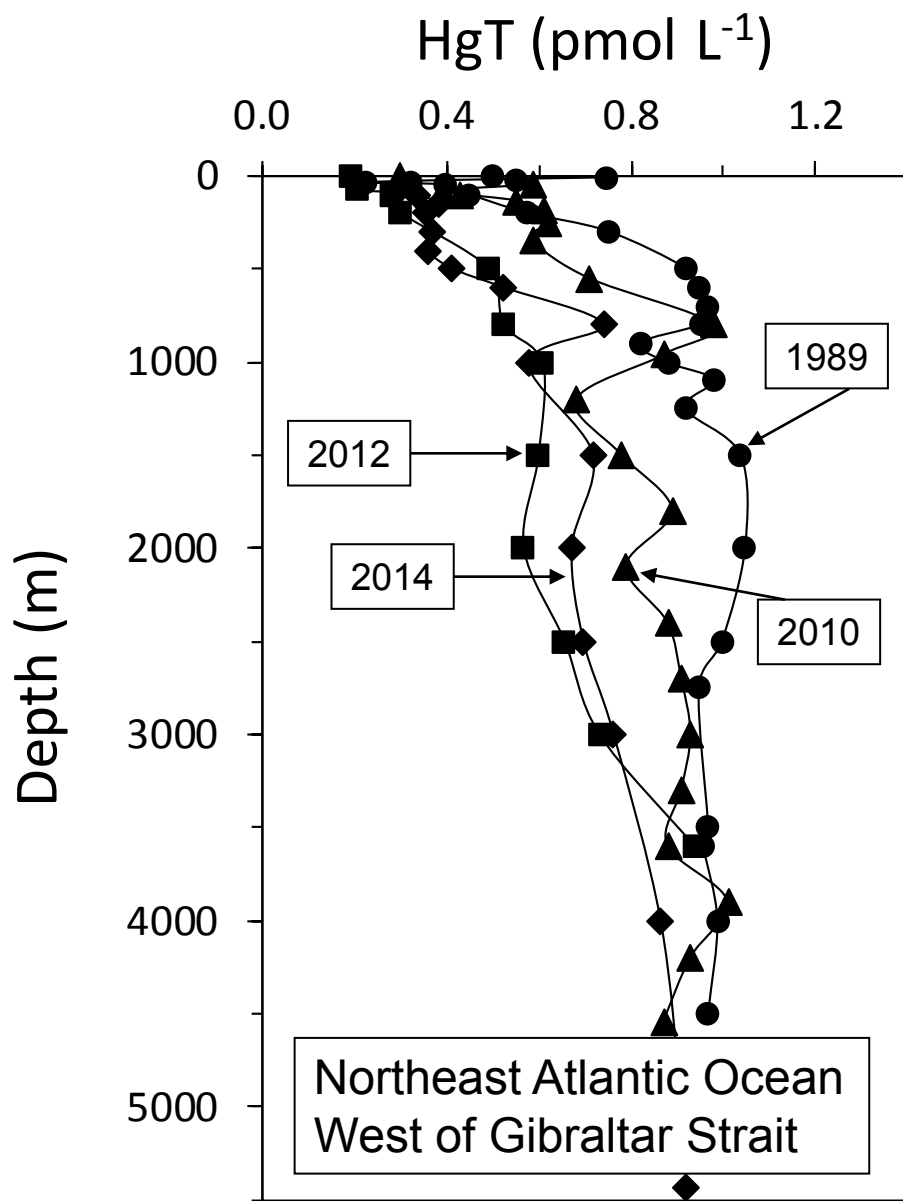


Fig. 6



1 Supplementary Information

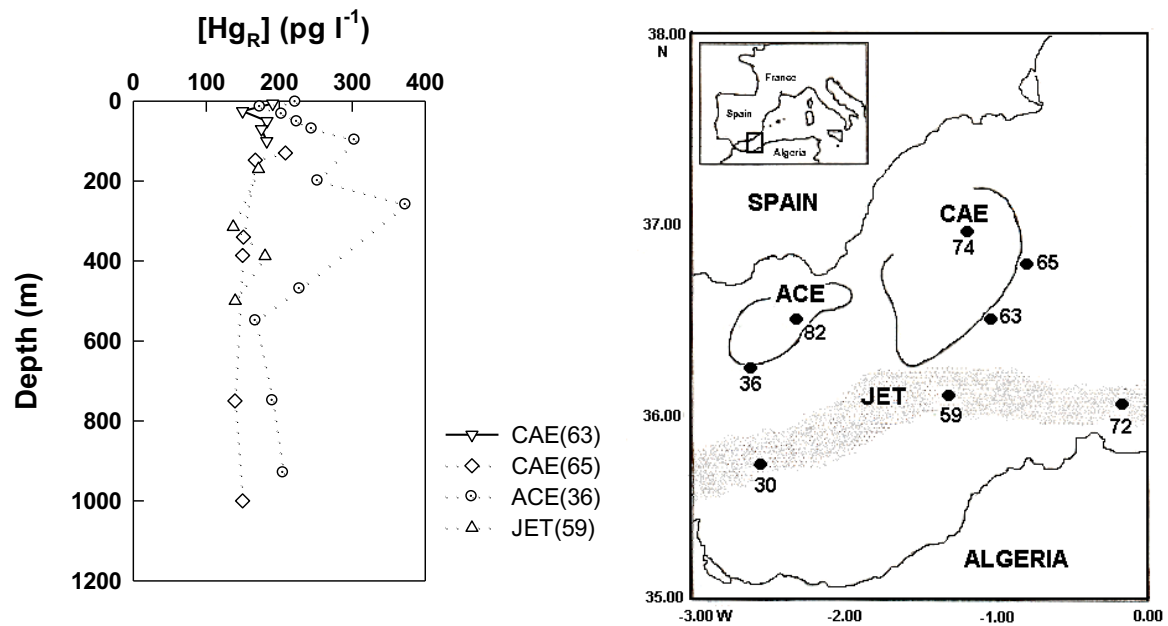
2

3 **SI 1.** Easily reducible Hg (HgR) distribution during the Almofront-I cruise in the Alboran Sea (1991).

4 Note that the relationship between HgR and total Hg (HgT) was linear between 200 and 1000 m ($R^2 =$

5 0.71), with a mean HgR/HgT ratio of 0.45; this ratio was used to extrapolate from HgR six missing

6 HgT concentration values at Sta. 36.

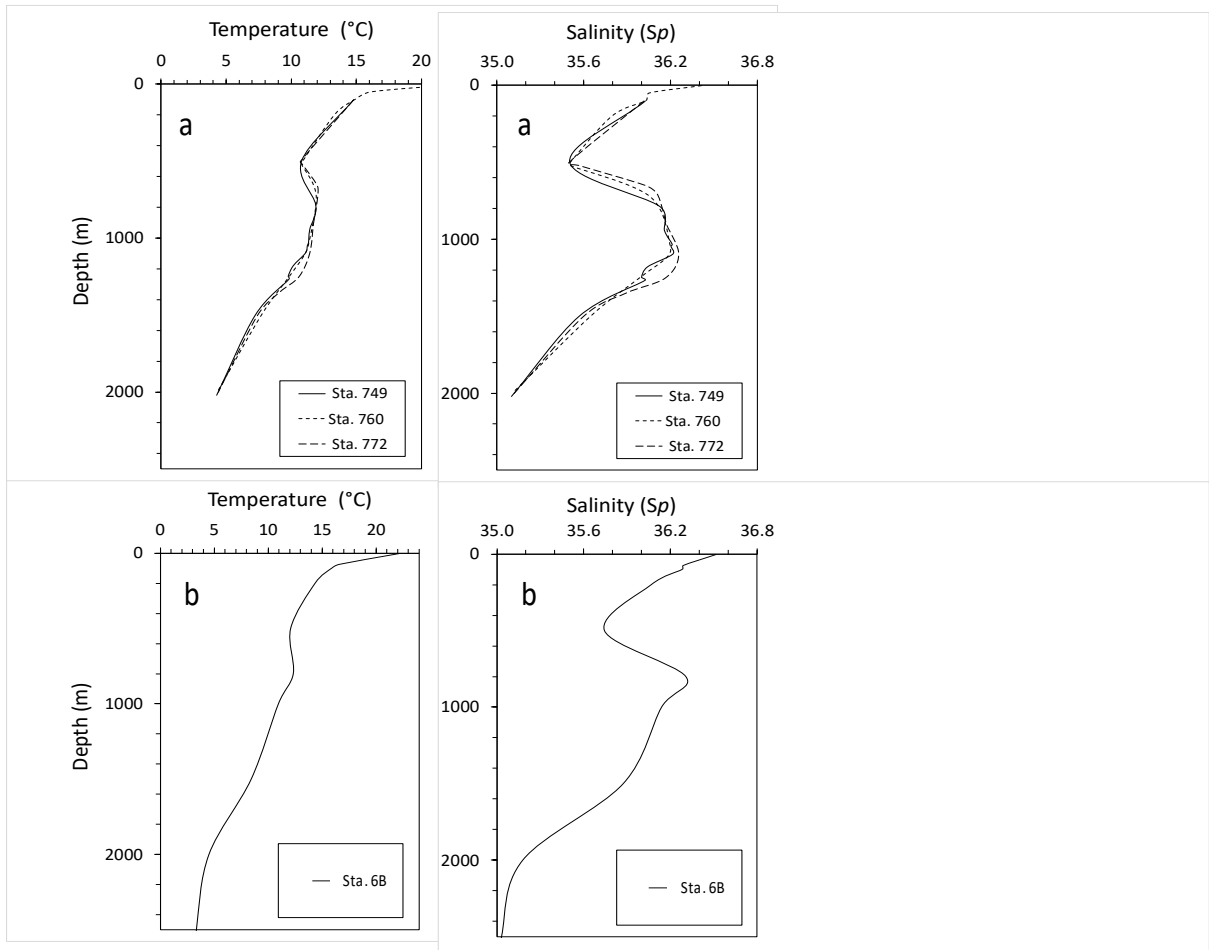


7

8

9

10 **Figure S1.** West of Gibraltar. Temperature and salinity profiles during the (a) MEDATLANTE-II cruise
11 (1989) at Stas. 749, 760 and 772 closed to Sta. 6A, and during the (b) FENICE cruise (2012) at Sta 6B.



12

13

14

15

16

17

18

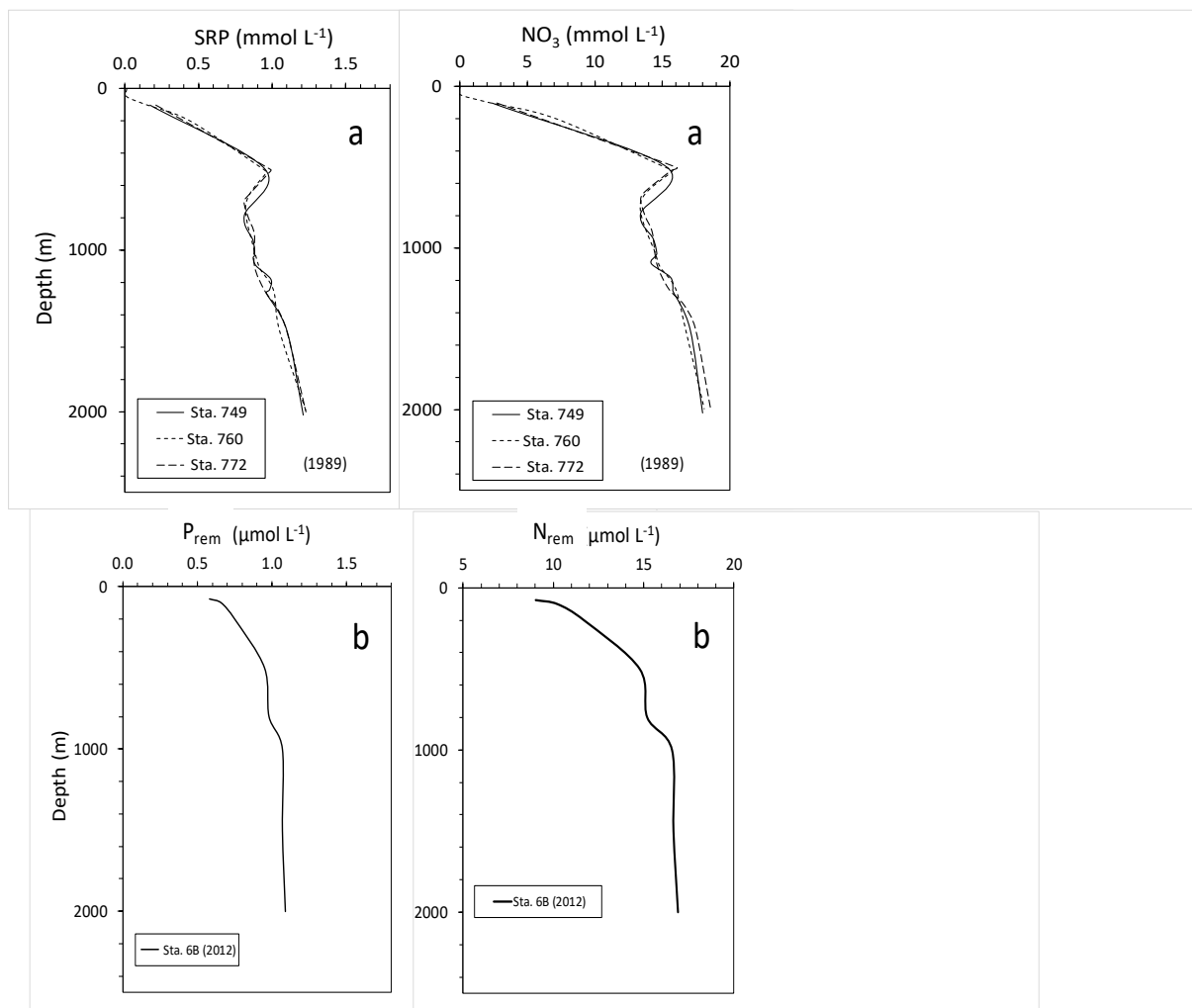
19

20

21

22

23 **Figure S2.** West of Gibraltar. Soluble Reactive phosphorus (SRP) and remineralized phosphorus
24 (P_{rem}) and nitrate (NO_3) and remineralized nitrogen (N_{rem}) profiles during the (a) MEDATLANTE-II
25 cruise (1989) at Stas. 749, 760 and 772 closed to Sta. 6A, and during the (b) FENICE cruise (2012) at
26 Sta 6B. The Redfield ratios used for $P_{rem}/N_{rem}/AOU$ are 1/17/141 according to Minster and Boulhadid
27 (1987).



28

29

30

31

32

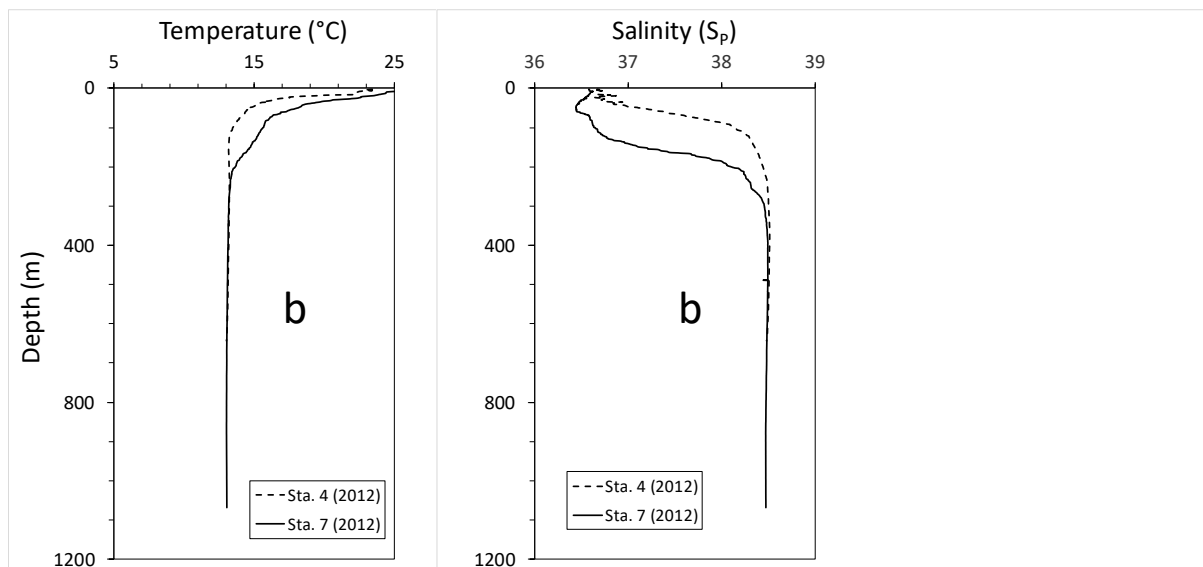
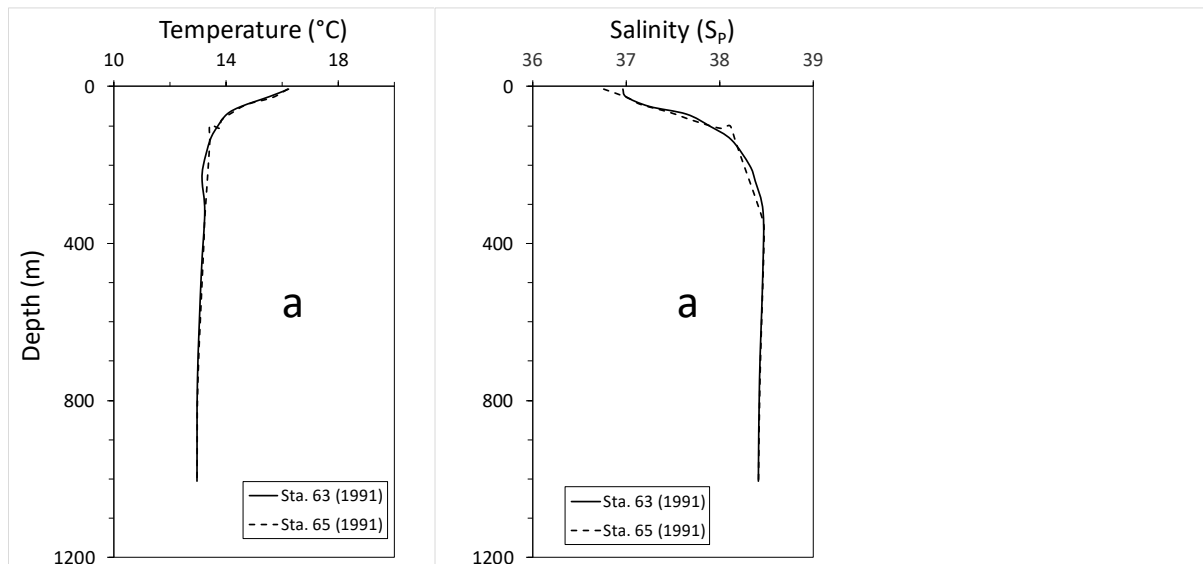
33

34

35

36 **Figure S3.** East of Gibraltar. Temperature and salinity profiles during the (a) ALMOFRONT-I cruise
37 (1991) at Stas. 63 and 65, and during the (b) FENICE cruise (2012) at Stas. 4 and 7.

38



39

40

41

42

43

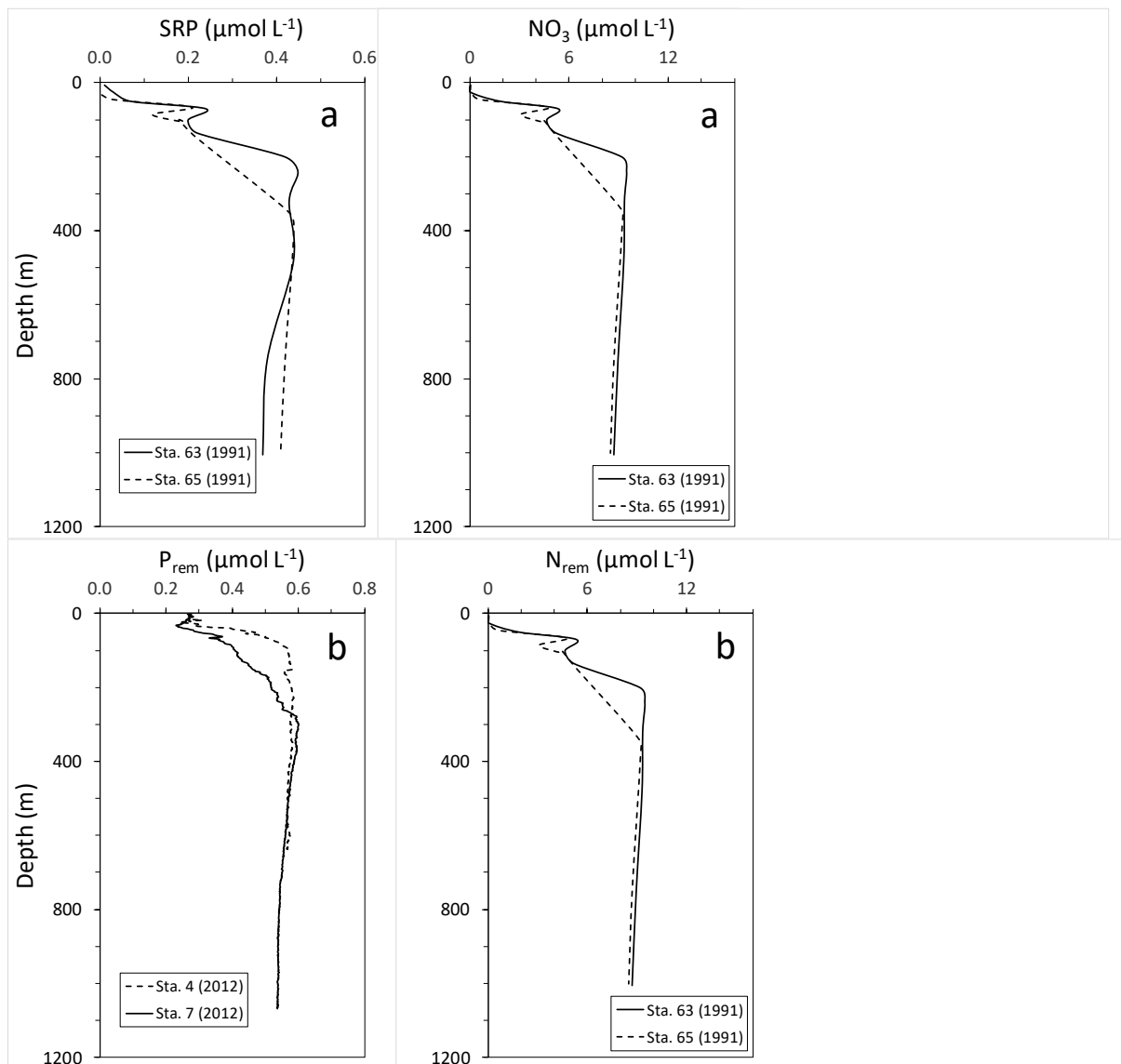
44

45

46 **Figure S4.** East of Gibraltar. Soluble Reactive phosphorus (SRP) and remineralized phosphorus (P_{rem})
47 and nitrate (NO_3) and remineralized nitrogen (N_{rem}) profiles during the (a) ALMOFRONT-I cruise
48 (1991) at Stas. 63 and 65, and during the (b) FENICE cruise (2012) at Stas. 4 and 7. The Redfield ratios
49 used for $P_{rem}/N_{rem}/AOU$ are 1/22/237 according to Béthoux et al. (2005).

50

51



52

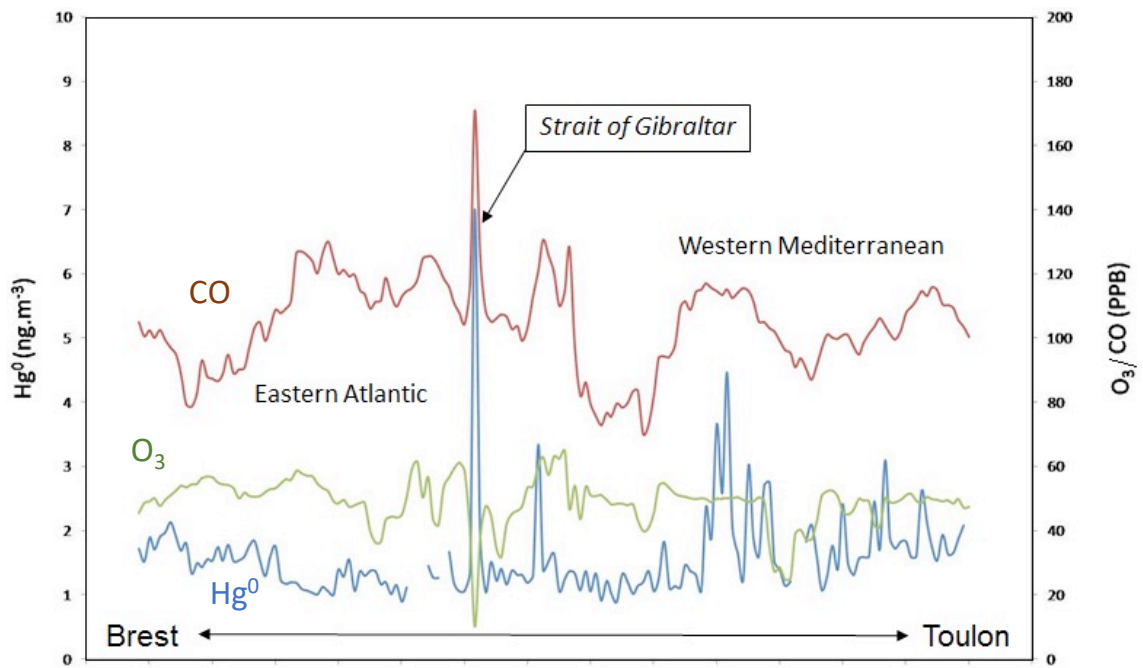
53

54

55

56

57 **Figure S5.** Hg concentrations, ozone and carbon monoxide in the atmosphere (10 m above the sea
58 level) during a transit between Toulon and Brest in April 2012.



59